FFI-rapport 2009/00155

A comparison of AUTODYN and RSPH on two-dimensional shock waves problems

Steinar Børve, Audun Bjerke, Marianne Omang [1], and Eirik Svinsås

Norwegian Defence Research Establishment (FFI)

2009-01-20

[1] Affiliation: Norwegian Defence Estates Agency (Forsvarsbygg), P.O. Box 405 Sentrum, 0103 Oslo, Norway

FFI-rapport 2009/00155

1120

P: ISBN 978-82-464-1493-5
E: ISBN 978-82-464-1494-2

Keywords

Sjokkbølge

Numerisk simulering

Detonasjo

Approved by

Eirik Svinsås	Project manager
Jan Ivar Botnan	Director

English summary

It is important, both to the military and civilian community, to be able to predict the strength and propagation pattern of shock waves generated from the detonation of high explosives. This report documents a comparative study of two different simulation tools, **AUTODYN** and **Regularized Smoothed Particle Hydrodynamics (RSPH)**, used in the study of shock waves in air. **AUTODYN** is a commercially available software based on several numerical solvers and has been used at FFI for quite some time. **RSPH**, based on the numerical method **Smoothed Particle Hydrodynamics (SPH)**, is a software package initially developed at the University of Oslo in collaboration with the Norwegian Defence Estates Agency. Over the last couple of years though, FFI has also provided a major contribution to the on-going development of the code. This development has been motivated by the general desire to accurately model nonlinear problems in fluid dynamics.

In this work we compare the numerical results obtained with **AUTODYN** and **RSPH** on two-dimensional shock problems. The tests assume either planar or cylindrical symmetry. The results from the two different software packages are to a large degree qualitatively similar, although quantitative differences occur. Furthermore, the study reveals a major difference in accuracy between the two solvers available in **AUTODYN** for treating this kind of problems. The more commonly used **Godunov** solver is shown to be substantially less accurate than the other two solvers. As for computational speed, **RSPH** seems to be roughly twice as fast as **AUTODYN**.

Sammendrag

Det er svært viktig, både i militær og sivil samanheng, å kunne forutsjå styrken og forplantingsmønsteret til sjokkbølgjer frå detonasjonar av høgeksplosiv. Denne rapporten dokumenterar ei samanliknande studie av to ulike simuleringsverkty, **AUTODYN** og **Regularized Smoothed Particle Hydrodynamics (RSPH)**, til bruk ved studie av luftsjokk. **AUTODYN** er ein kommersielt tilgjengeleg programvare basert på fleire ulike løysingsmetodar, og har i lengre tid har vorte brukt på FFI til mellom anna å studere luftsjokk. **RSPH**, basert på løysingsmetoden **Smoothed Particle Hydrodynamics (SPH)**, er ein programvare som opprinneleg vart utvikla ved universitetet i Oslo i samarbeid med Forsvarsbygg. I dei seinaste par åra, har óg FFI gjeve viktige bidrag til vidareutviklinga av koden. Denne utviklinga har vore motivert av eit generelt ønske om nøyaktig å kunne modellere ikkje-lineære problem i fluiddynamikken.

I dette arbeidet samanliknar vi numeriske resultat frå simuleringar med **AUTODYN** og **RSPH** på todimensjonale sjokkproblem. Testane antek anten plan eller sylindrisk symmetri. Resultata frå dei to ulike programma viser stor grad av kvalitativt samsvar, jamvel om det finst ein del kvantitative skilnader. Vidare viser studia at dei to løysingsmetodane i **AUTODYN** som er aktuelle for denne type problem, gjev høgst ulik nøyaktighet. **Godunov**-løysaren, som er den mest vanleg brukte løysaren, har vist seg å vere langt mindre nøyaktig enn dei to andre løysarane. Når det gjeld reknefarten på dei to programvarane, ser det ut til at **RSPH** er opptil dobbelt så rask som **AUTODYN**.

Contents

1 Introduction

It is important, both to the military and civilian community, to be able to predict the strength and propagation pattern of shock waves generated from the detonation of high explosives. An example of this is the need to estimate the necessary safety range around ammunition storage facilities. The nonlinear character of such problems often makes analytic methods inadequate tools in obtaining accurate estimates in complex geometries. Instead, one normally needs to use a combination of high-quality experiments and accurate numerical models. Since relevant experiments often will be both highly time-consuming and costly, being able to accurately simulate detonation processes and shock wave propagation numerically is of utmost importance in increasing our understanding of such problems. In pursuit of accurate simulation results we need to improve both the underlying physical models as well as the numerical techniques used to solve the equations which represent the models. An example of how difficult it might be to reproduce experimental results, is the simulations of detonation inside an underground ammunition storage facility performed at FFI by Teland and Wasberg [22]. They report simulated peak pressure values that are roughly 2.5-5.0 times higher than the measured peak pressure values for a detonation charge consisting of 10000kg TNT. It is uncertain whether the large deviation is caused mainly by errors in the physical model or in the numerical interpretation of the model.

In this work we focus on aspects of different numerical models, while keeping the physical model fairly simple. This is done by comparing the solutions from two widely different numerical codes on problems which involve the detonation of high explosives in two-dimensional geometries, either planar or cylindrically symmetric. The high explosives (HE) are modelled using the constant volume description, rather than using the commonly favoured JWL equation of state of TNT-profiles [16]. In the current description, the HE are assumed to have been instantaneously transformed into hot, dense ideal gas. With this assumption, a single-fluid model can be used. The two codes to be compared in this study are the commercially available software **AUTODYN** and the academically developed method **Regularized Smoothed Particle Hydrodynamics (RSPH)**.

1.1 Model equation

The governing equations for the evolution of a non-viscous, ideal fluid can be written on integral or differential form, based on a Eulerian or Lagrange description. For the case of an Eulerian description on differential form, we have:

$$\frac{\partial \rho}{\partial t} + \boldsymbol{\nabla} \cdot (\rho \boldsymbol{v}) = 0, \tag{1.1}$$

$$\frac{\partial (\rho \boldsymbol{v})}{\partial t} + \boldsymbol{\nabla} \cdot (\rho \boldsymbol{v}\boldsymbol{v}) = -\boldsymbol{\nabla} p, \tag{1.2}$$

$$\frac{\partial (\rho e)}{\partial t} + \boldsymbol{\nabla} \cdot (\rho e \boldsymbol{v}) = -p \boldsymbol{\nabla} \cdot \boldsymbol{v}, \tag{1.3}$$

with the additional constraint given by the adiabatic equation of state

$$p = (\gamma - 1)e\rho. \tag{1.4}$$

Equations 1.1-1.3 can be rewritten for the Lagrangian case by using the Lagrangian derivative $D/Dt = \partial/\partial t + \boldsymbol{v} \cdot \boldsymbol{\nabla}$ as follows:

$$\frac{D\rho}{Dt} = -\rho(\boldsymbol{\nabla} \cdot \boldsymbol{v}), \tag{1.5}$$

$$\frac{D\boldsymbol{v}}{Dt} = \frac{\boldsymbol{\nabla} \cdot p}{\rho}, \tag{1.6}$$

$$\frac{De}{Dt} = -\frac{P}{\rho}(\boldsymbol{\nabla} \cdot \boldsymbol{v}). \tag{1.7}$$

The latter formulation is in many respects simpler than the former and is appropriate when describing the evolution of the system as seen by an observer following the fluid flow.

1.2 AUTODYN

AUTODYN was developed by **Century Dynamics** but is now part of the **ANSYS Workbench Platform**. The software has been widely used at FFI since 1997, see e.g. [2]. It is an explicit hydrocode that includes several different solvers, including Euler (both **Godunov** and **FCT**), Lagrange, Arbitrary Lagrange Euler, Smoothed Particle Hydrodynamics, Shell, and Beam. Each solver has its strengths and weaknesses and is suitable for solving a certain range of problems. When modelling shock waves one would use an Euler solver, either Godunov or FCT (Flux-Corrected-Transport). The Godunov method reaches a solution by solving the local Riemann problems at all cell interfaces [9]. The FCT method has an additional *anti-diffusion* step which, as the name implies, corrects for the numerical diffusion otherwise introduced in the numerical solution [3]. Combined with an extensive material model library, and a user-friendly, graphical interface, this makes AUTODYN a versatile numerical tool. But like any other piece of software, AUTODYN has its shortcomings. When studying shock wave effects, the more important issues with AUTODYN seems to be

- The software has an upper limit on the number of calculation nodes of about $4 \cdot 10^6$. Pre- and post-processing on a standard PC seems at present to reduce the maximum number of calculation nodes to about $1 \cdot 10^6$ in practical situations [2].
- The Euler solvers are not adaptive. This means that the code cannot automatically change node size in time and space to better adapt to the dynamics of the problem. This is a feature which in the last 10-15 years have been introduced in many numerical codes dealing with hydrodynamical problems to reduce CPU-time and memory use in two- and three-dimensional modelling.
- Despite the impressive range of solvers found in AUTODYN, it might be difficult to handle certain sub-classes of problems. One such sub-class involves the interaction between shock

waves in gas and easily fragmented solids. The former phase one would describe in AUTODYN by an Euler solver, the latter phase can only be handled properly by SPH (or similar methods). Unfortunately, no coupling techniques exist in the current version of AUTODYN between the Euler solvers and SPH.

- Much research is still needed in order to properly understand the physics of detonation processes and shock wave propagation in non-ideal media. When trying to understand the fundamental mechanisms of a physical problem through the use of numerical simulations, it is important that the researcher is free to modify and adjust the numerical code as deemed necessary. With AUTODYN, the possibilities for performing modifications is limited.

- With a small number of licences available, managed through an online authentication procedure, the access to the software is restricted. This can potentially represent a bottleneck in the daily workflow causing unnecessary delays in the research. This can in particular be the case if several time-consuming simulations are required to run simultaneously.

1.3 Regularized Smoothed Particle Hydrodynamics (RSPH)

Regularized Smoothed Particle Hydrodynamics (RSPH) is different from AUTODYN in almost every aspect, except that this method is also designed to handle non-linear problems in fluid dynamics. The method is an extension to the meshless method **Smoothed Particle Hydrodynamics (SPH)** [14]. (SPH is also included as a solver in AUTODYN. However, the SPH solver in AUTODYN is not suitable for studying shock waves in compressible fluids due to the way the method has been implemented there.) SPH was originally developed for handling gas dynamics in astrophysical applications characterized by large variations in density and free surface boundaries [8]. Later on, SPH has found good practical use in the study of highly deformed or fragmented solids [1] and free surface water waves [6]. The method is Lagrangian, meaning that the computational nodes, referred to as particles, move with the fluid flow. This implies that the node density which inevitably controls the resolution of the description will in general be varying both in time and space. The method is very robust when it comes to coping with highly irregular particle distributions, at the expense of reduced accuracy and possibly also efficiency. The standard SPH method is therefore not considered particularly well suited for studying shock wave phenomena.

RSPH was developed, both as a method and a code, at the University of Oslo [4, 5]. What distinguishes RSPH from the more standard SPH method, is the flexibility with which the resolution can be made adaptive, and the regularization technique introduced to prevent the particle distribution from becoming too irregular. In contrast to what is the case with standard SPH, resolution no longer needs to be a function of the initial particle distribution and the subsequent, time-dependent flow pattern. RSPH is able to maintain high resolution in regions of interest, for example near shock wave structure, and low resolution elsewhere. Comparisons with experiments, e. g. [16, 17], have shown good accuracy in simulating shock waves generated by detonating high explosives. Through a regularization process performed at suitable time intervals, the numerical description is re-evaluated to

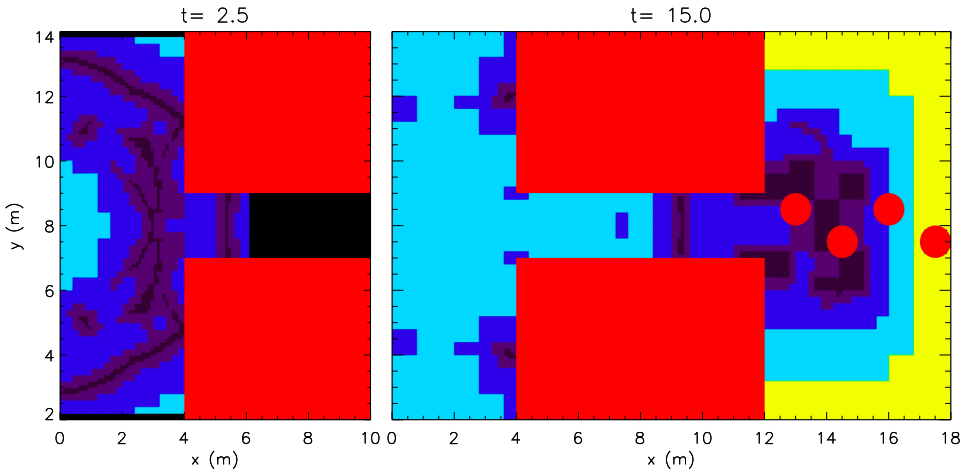

Figure 1.1: Colour maps of the resolution profile at two points in time (t=2.5 and t=15.0) for a typical simulation of the plane chamber test described in chapter 3.

achieve a more optimal description as well as to remove unwanted irregularities in the particle distribution. Combined with the capability of handling free surfaces, inherited from standard SPH, the adaptive nature of RSPH makes the code ideal for studying multi-dimensional shock wave propagation in an ambient medium. In figure 1.1 this is illustrated by colour maps of the resolution profile at two points in time (t=2.5 and t=15.0) for a typical simulation of the plane chamber test described in chapter 3. Brighter colours mark low resolution regions, relatively speaking, while the darker colours mark the high resolution region. The red coloured regions are outside the computational domain. An exception to these colouring rules is found in the regions defined by $y < 2.2$m, $y > 13.8$m, and $x > 6$m at t=2.5ms. Black colouring in these regions indicate that no particles have yet been generated here and that the ambient gas condition is assumed to apply.

Having first hand knowledge about and access to a reliable numerical code is of vital importance when trying to investigate which mechanisms can, under various conditions, be important to the description of detonation processes and shock wave propagation. One good way of achieving this is to build a code from scratch. There are however several valid objections that can be raised against developing and maintaining a non-commercial code. In the particular case of the RSPH code, objections that can be raised against using the code are for instance:

- Although the main functionality of the code has already been developed, maintenance and further developments still takes time. It will usually be a more time-consuming approach than relying purely on commercial software. Extending the functionality of the code include e.g. solids will require a considerable programming effort.

- To fully utilize the adaptive features of RSPH one is required to have a fairly in-depth knowledge of how the code works. The learning curve is therefore rather steep.
- Since RSPH is based on SPH, which usually is considered a relatively slow method when modelling shock waves, an adaptive mesh code could be a faster option. To the extent that adaptive mesh based codes are commercially available, this might be an even better option.
- Setting up a new problem may take longer since no library of predefined materials is available.

1.4 Outline of the work

The rest of the report is devoted to presenting simulation results from one- and two-dimensional tests made by using either the RSPH code, the Godunov solver of the AUTODYN code, or the FCT solver of the AUTODYN code. In chapter 2 we focus on two simple, idealized tests which in reality can be formulated in one dimension. These tests have the benefit of being widely used in the literature, and comparisons can therefore be made against known solutions. In chapter 3 we look at truly two-dimensional problems in plane symmetry. We discuss the ability of the codes to describe Richtmyer-Meshkov instabilities naturally occurring in these types of problems. We also present results from simulation of a detonation in a fairly complex, plane symmetric chamber. This test also illustrates how well solid boundaries are treated in the two codes. Results from the simulation of a cylindrically symmetric chamber with a barrier in front of the tunnel opening is described and compared in chapter 4. Through these tests we will show that the difference between the two AUTODYN (Godunov and FCT) results in most cases are larger than the difference between the RSPH results and the AUTODYN FCT results. Why this is important to note is discussed in the final chapter, chapter 5.

2 One-dimensional tests

In this chapter we present results from simulations of two tests that exhibit spatial variation only in one dimension. The AUTODYN code has represented this as a one-dimensional chain of grid cells. The RSPH code solves the problem in a truly two-dimensional domain, but where the domain extent perpendicular to the x-axis is much less than unity. CPU times have therefore not been compared for these two cases. Instead, we compare accuracy and the number of computational nodes in a one-dimensional chain.

2.1 Strong shock with extreme jumps in pressure and velocity

The first test is in [24] described as a severe problem to test not only in terms of numerical stability and robustness, but also when it comes to conservation of the numerical method. In fact, non-

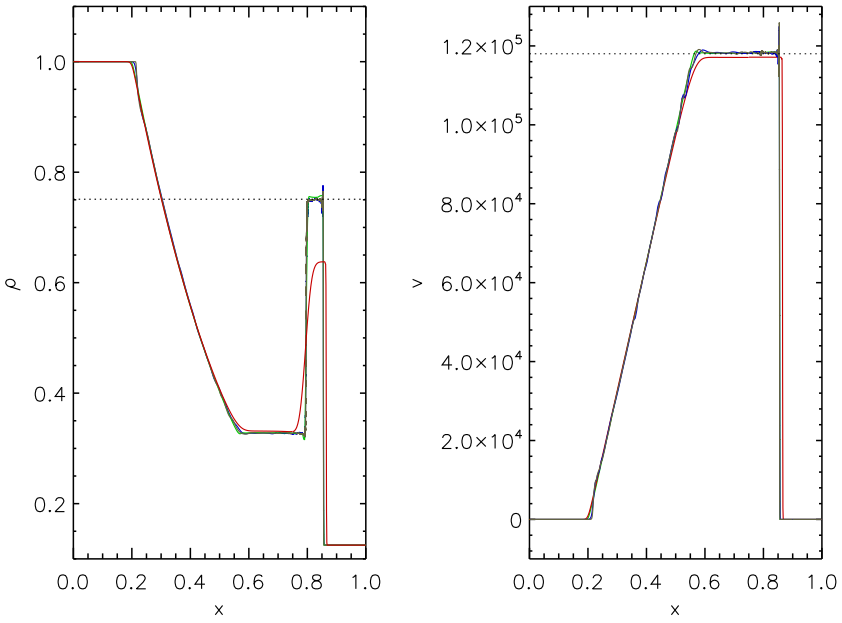

Figure 2.1: *Density (left) and velocity (right) profiles for the extreme shock test at $t = 2.5 \times 10^{-6}$. We have plotted the 4 compared solutions obtained with the AUTODYN Godunov solver (red), the AUTODYN FCT solver (green), the RSPH solver with $< n_p > \approx 570$ (blue) and $< n_p > \approx 840$ (grey).*

conservative schemes tend to produce incorrect shock positions, especially in the case of strong shocks. The initial condition is defined within the computational domain $0 \leq x \leq 1$ and consists of a left and right hand state separated by a membrane at $x = 0.5$. The initial state vector $\boldsymbol{q} = (\rho, v, P)$ can be written in dimensionless units as

$$\boldsymbol{q} = \begin{cases} (1.0, 0.0, 1.0 \times 10^{10}) & \text{for } 0 \leq x \leq 0.5 \\ (0.125, 0.0, 0.1) & 0.5 < x \leq 1.0. \end{cases} \tag{2.1}$$

This initial condition creates a supersonic shock.

The problem is solved using AUTODYN with either the Godunov or FCT solvers, both utilizing 1000 grid points uniformly placed in a one-dimensional row structure. The RSPH code was run twice, in both cases utilizing a non-uniform, non-static particle distribution. The time averaged particle number along the x-axis was $< n_p > \approx 570$ and $< n_p > \approx 840$, respectively, in the two simulations. In Figure 2.1 we have plotted the density and velocity for all the 4 different simulations at time $t = 2.5 \times 10^{-6}$. The red and green curves correspond to the Godunov and FCT solutions, respectively, while the blue and grey represent the two RSPH solutions. In addition to the 4 numerical solutions, we have plotted a straight, dotted line in both plots indicating the correct density and velocity level in the approximate intervals $0.8 < x < 0.85$ and $0.6 < x < 0.85$, respectively, as given in [24].

First, we notice how the Godunov solution deviates substantially from the other 3 solutions. The local maximum in density is generally underresolved and, more specifically, underestimated by roughly 16%. Also the top velocity is underestimated. In addition, the strong shock has moved faster in the Godunov solution, possibly indicating a lack of conservation. As for the other 3 solutions, only minor differences separate them. If we look closely, we see that the green curve in the density plot representing the FCT solution is situated slightly above both the two RSPH solutions as well as the correct level indicated by the dotted line in the interval $0.8 < x < 0.85$. In contrast, both the two RSPH solutions reveal some overshoot at the strong shock position at $x \sim 0.85$. Apart from this, all 3 solutions can be said to be highly accurate. It is however noticeable that the lower resolution RSPH simulation achieves this with a more than 40% reduction in computational nodes compared to that used by the AUTODYN FCT solver.

2.2 Two interacting blast waves

A much used test problem describing the interaction of two blast waves was proposed by Woodward and Colella in 1984 [23]. It involves multiple interactions of strong shocks and rarefaction waves with each other and with discontinuities. The gas is initially at rest in the interval $0 \leq x \leq 1$ with reflecting boundary conditions on either sides. The initial density ρ is 1 throughout the interval. The blast waves are driven by two large steps in the pressure profile according to the expression

$$P = \begin{cases} 1000 & \text{for } 0 \leq x \leq 0.1 \\ 0.01 & \text{for } 0.1 < x \leq 0.9 \\ 100 & 0.9 < x \leq 1.0. \end{cases} \tag{2.2}$$

Notice the asymmetry which is built into the problem as the two pressure jumps are not identical. The analytic solution to this problem is not known, but high resolution results obtained with codes based on finite difference calculations on a nonuiform Eulerian mesh have been presented [23]. The density and velocity profiles at 3 different points in time are shown in Figure 2.2. Just as in the previous case, 4 different solutions are plotted. The Godunov (red) and the FCT (green) solutions are obtained with 1000 uniformly distributed grid points. The two RSPH solutions use time-averaged particle numbers of $< n_p > \approx 750$ (blue) and $< n_p > \approx 900$ (grey), respectively.

The two blast waves are seen to propagate into the intermediate low pressure gas. At the same time, rarefaction waves form and propagate outward toward the boundaries, where they are reflected. The difference in the left and right hand blast wave Mach numbers causes the difference in shape of the shock profiles, as seen at $t = 0.016$. The shocks collide at $t = 0.28$ creating an extremely sharp density peak. The reflected rarefaction waves have by this time caught up with the shocks and weakened them. The profiles at $t = 0.038$ are a result of multiple interactions of strong nonlinear continuous waves and a variety of discontinuities. Just as in the previous case, the Godunov solution is the less accurate of the 4 solutions. This is mostly revealed by the lower fluid velocities and the errors in the shock positions, the latter applies in particular to the rightmost strong shock. The peak

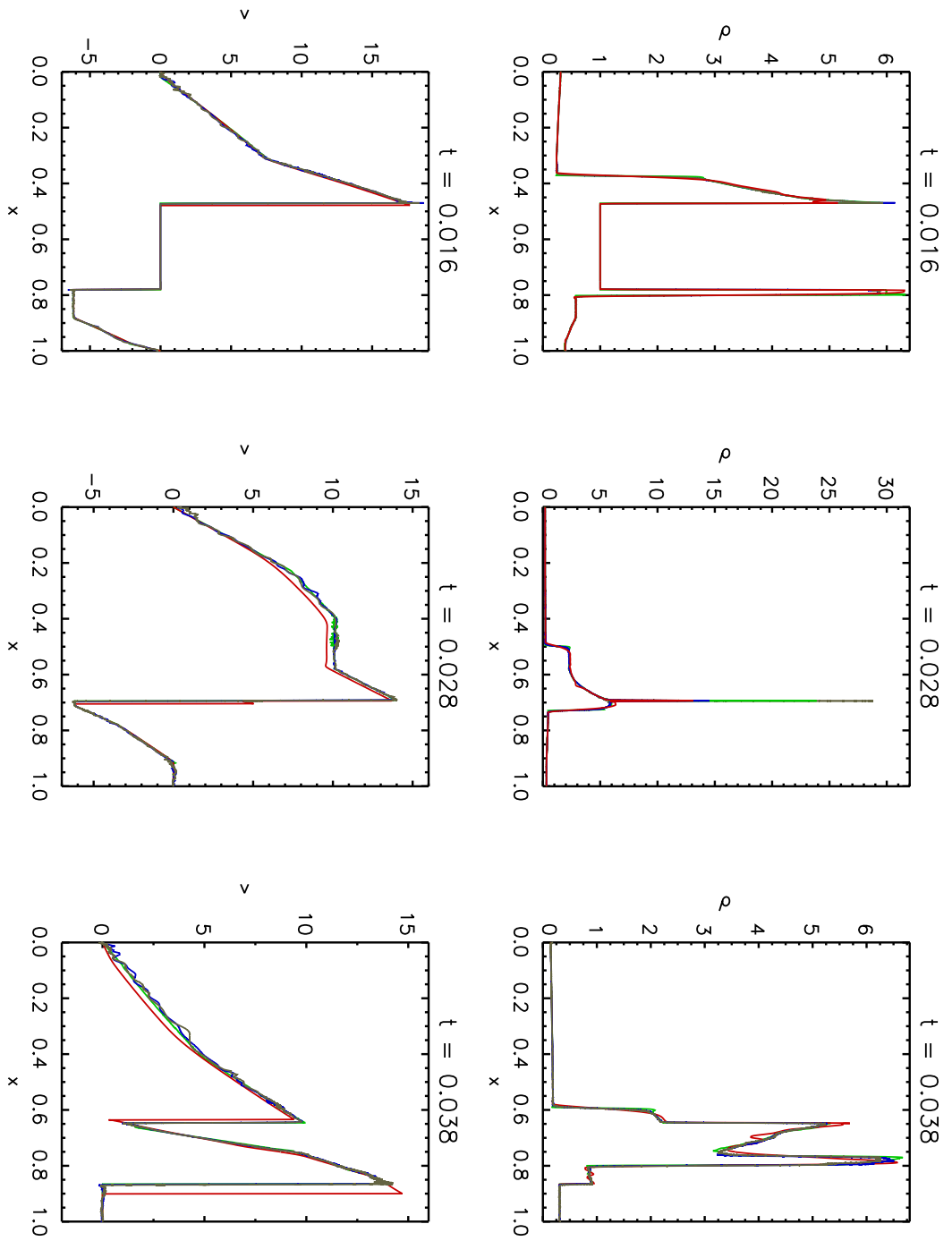

Figure 2.2: Density (left) and velocity (right) profiles for the two interacting blast waves test at 3 different points in time. We have plotted the 4 compared solutions obtained with the AUTODYN Godunov solver (red), the AUTODYN FCT solver (green), the RSPH solver with $< n_p > \approx 750$ *(blue) and* $< n_p > \approx 900$ *(grey).*

level at $t = 0.28$ is much too low, less than half the value reported in [23]. The peak level is not much higher in the first of the two RSPH solutions (blue), despite the fact that the solution elsewhere is highly consistent with the FCT and second RSPH solutions.

It might seem odd that the modest increase in the time-averaged particle number from 750 to 900 reduces the error in the peak density level at $t = 0.28$ from roughly 50% to practically 0 (compared to [23]). This is because the second solution has allowed the resolution to be increased additionally when the blast waves collide. This increase is only applied in a restricted region in space and for a short interval in time. Apart from this single difference, the two RSPH solutions are more or less identical. This illustrates nicely how the adaptive nature of the code can be utilized to improve accuracy at critical points in time and space at low cost. The FCT solution once again fits better with the RSPH solutions than what is the case with the Godunov solution. The peak level at $t = 0.28$ is quite high considering that a uniform grid is used. This is due to the FCT technique of compensating for the inherent numerical diffusion in grid codes, giving higher peak values than what would otherwise be possible to achieve.

3 Two-dimensional, plane symmetric tests

In this section we will consider a cylindrically shaped charge, described in a two-dimensional, plane symmetric model. The charge is assumed to consist of TNT with a mass density of $1630\text{kg}/\text{m}^3$ and a specific energy of 4.29MJ/kg. These material properties correspond to the TNT-2 model in the AUTODYN material library. The charge has an initial radius of 52.7mm and is surrounded by air with an assumed density of $1.293\text{kg}/\text{m}^3$ and a pressure of 1 atm. We will consider this charge in two different scenarios. The first problem is a close-up scenario where we look at the near-field description with a particular attention to Richtmyer-Meshkov instabilities [10, 25]. The second problem consider the propagation of shock waves generated by this charge in a larger, more complex chamber.

3.1 Richtmyer-Meshkov instabilities

The instability of a material interface under the acceleration of an incident shock was predicted theoretically by Richtmyer in 1960 [19] and experimentally confirmed by Meshkov ten years later [13]. The phenomenon, closely related to the Rayleigh-Taylor instability [21], is now known as the **Richtmyer-Meshkov** (RM) instability. This instability contributes to the mixing of materials, which in turn can lead to interactions between different layers of material. Such mixing processes can be important in describing chemical reactions occurring when detonating high explosives. Other areas of physics where this can be important is in inertial confinement fusion and supernova explosions [20]. Several theoretical, numerical, and experimental studies have therefore been devoted to the phenomenon [10, 12, 20, 25]. The basic mechanism of the RM instability is illustrated by Figure 3.1

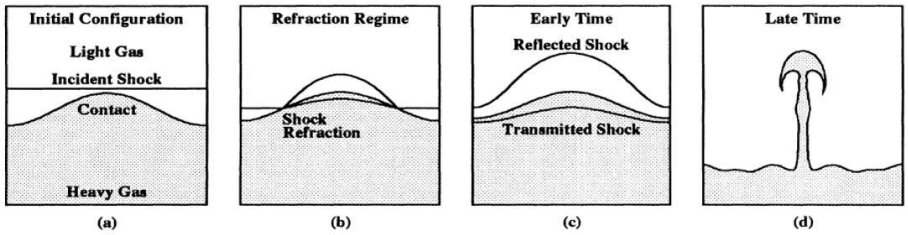

Figure 3.1: A schematic illustration of the mechanism behind the Richtmyer-Meshkov instability. Taken from [25].

taken from [25]. A shock interacts with a material interface, e. g. contact discontinuity. As a result, the shock is separated into a transmitted and a reflected wave. The interface itself is accelerated in such a way that any perturbations on the interface grows.

The initial condition of this test is in principle cylindrical. However, RM instabilities are expected to allow small perturbations to grow and thereby destroy the symmetry. (In real life experiments, small deviations from perfect symmetry will always exist. This is also the case in numerical descriptions.) A one-dimensional, cylindrical description is therefore not valid if you want to capture mixing processes naturally occurring during the detonation of HE. To reduce the computational cost, we do however assume that the angular variations can be sufficiently described by looking at one quadrant of the full, cylindrical problem. The problem was run for 1ms with 4 different resolutions of each of the three solvers. In AUTODYN, the problem is solved in a 2m by 2m region using 200×200 (run **a**), 400×400 (run **b**), 800×800 (run **c**), and 1000×1000 (run **d**) grid cells, using either the Godunov or the FCT solver. In RSPH the problem is solved in a 4m by 4m region. However, when performing regularization particles are only placed within a circular sub-domain. The radius of this sub-domain must be chosen so that any perturbations caused by the detonation do not propagate all the way to the boundary of the modelled sub-domain before the next regularization is performed. The smallest allowed particle size in the 4 RSPH simulations is 10mm (run **a**), 5mm (run **b**), 2.5mm (run **c**), and 1.25mm (run **d**). The test described in this section has also been used in a recent study [11]. There, the computations used wedge shaped grid cells which gradually expanded radially from an initial resolution ranging from 0.2mm to 0.8mm. The problem was run on a 25 processor Linux cluster. This represents a high-resolution reference solution.

Immediately after detonation, an initial shock propagates outward sweeping up ambient gas and thereby increasing the air density by roughly a factor 4 and the thermal pressure by nearly a factor 100. Behind the initial shock, a contact discontinuity evolves. It is small irregularities on this discontinuity front that grow due to the RM instability. In Figures 3.2 and 3.3 we show the density profile at t=0.35ms as found by the RSPH and FCT solvers, respectively. The figures illustrate from the top left panel to bottom right panel, the solutions for the runs **a-d**. The characteristic, finger-like structures caused by the RM instability can already be seen. We also note that an increase in resolution causes the fingers to become longer and thinner. The RSPH solutions reveal relatively large growth rates with a fairly uniform angular distribution of fingers. Small-scale noise is visible

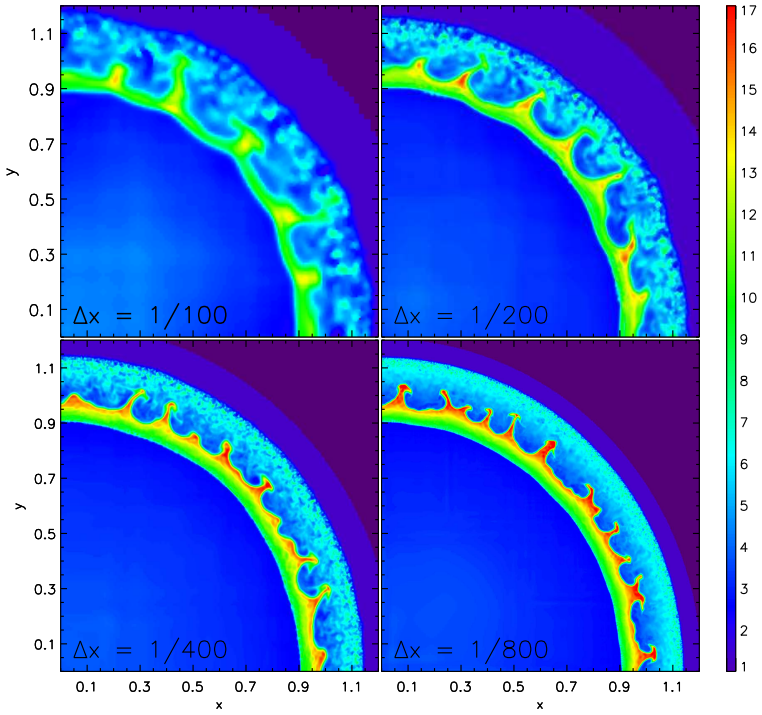

Figure 3.2: Density profiles produced by the RSPH solver in the Richtmyer-Meshkov test at t=0.35ms. Shown from the top left panel to the bottom right panel are the solutions from **a**-**d**.

at the initial shock front. In the case of FCT, the fingers grow more slowly. The finger structures are mostly found near the diagonal. Neither the RSPH results nor the high resolution results presented in [11] show any indications of an angle dependent growth rate for the instability structures. More likely, the FCT results show signs of what could be an increased numerical viscosity near the boundaries. In other words, this is probably a non-physical feature of the FCT solver.

A similar overall picture is seen in Figures 3.4 and 3.5 showing the RSPH and FCT density profile, respectively at t=0.80ms. The finger-like structures in Figure 3.4 are thinner and longer than the corresponding structures in Figure 3.5. The resolution study in [11] finds the finger-like structures to become thinner, longer, and more irregularly shaped as resolution is increased. Figures 3.4 and 3.5 can therefore be interpreted as indicating a higher effective resolution in the RSPH results than in the corresponding FCT results. The angular distribution of fingers in the FCT solutions are still to some extent anisotropic. Nevertheless, the RSPH and FCT results can be said to be largely consistent with each other and with the results in [11]. The Godunov results on the other hand, are distinctly different from the other results. Figure 3.6, which shows the Godunov solution at time t=0.80ms, exhibit no traces of any instabilities. In fact, the solution is very smooth with negligible deviations from cylindrical symmetry. This shows that the Godunov solver is not capable of capturing these small-scale phenomena, presumably because the level of numerical dissipation is too high.

To be able to study the differences between the solutions found by the three solvers more closely, we wanted to record the temporal variations of density and pressure at a given point in space. One

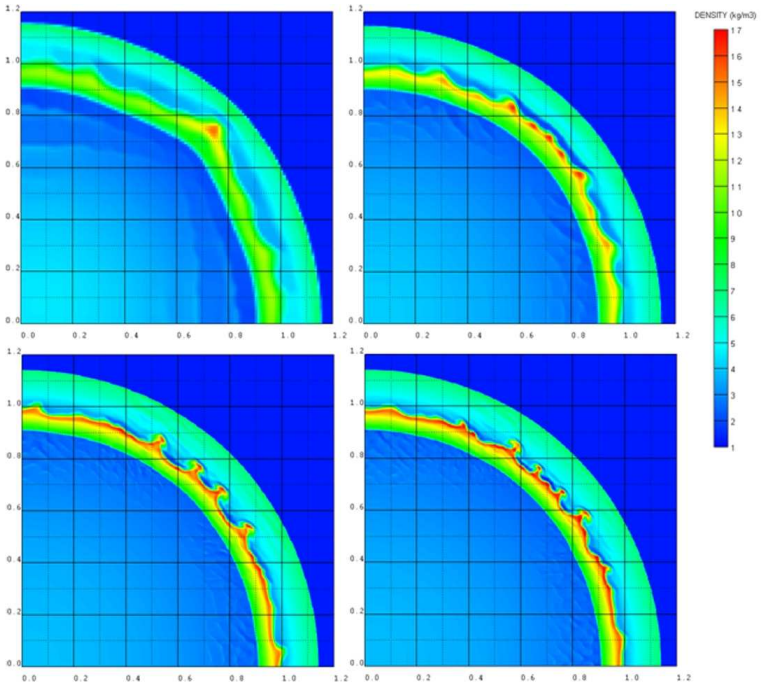

Figure 3.3: Density profiles produced by the FCT solver in the Richtmyer-Meshkov test at t=0.35ms. Shown from the top left panel to the bottom right panel are the solutions from **a-d**.

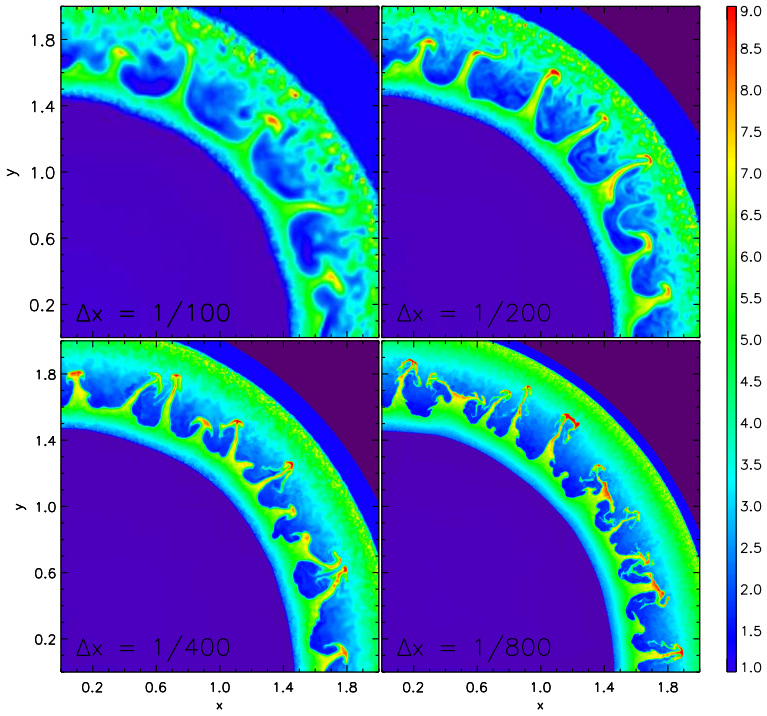

Figure 3.4: Density profiles produced by the RSPH solver in the Richtmyer-Meshkov test at t=0.80ms. Shown from the top left panel to the bottom right panel are the solutions from **a-d**.

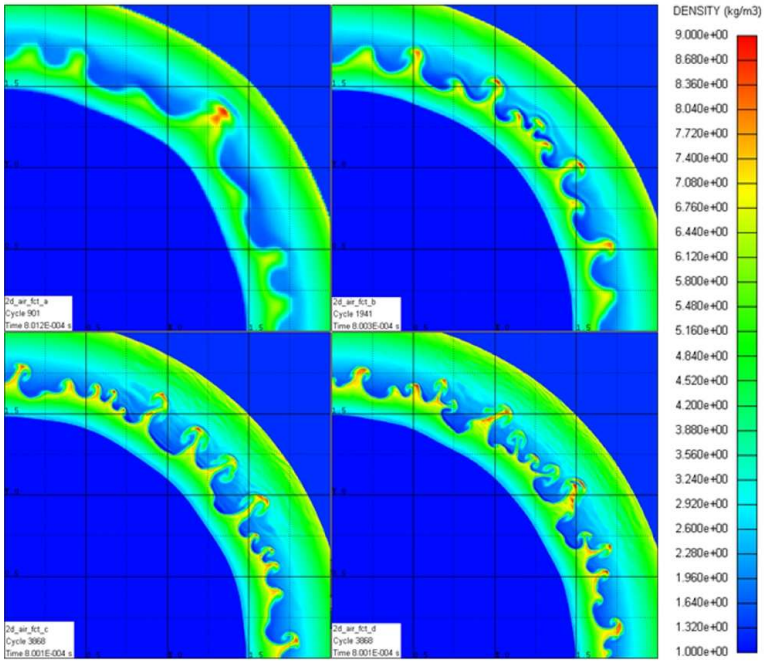

Figure 3.5: Density profiles produced by the FCT solver in the Richtmyer-Meshkov test at t=0.80ms. Shown from the top left panel to the bottom right panel are the solutions from **a-d**.

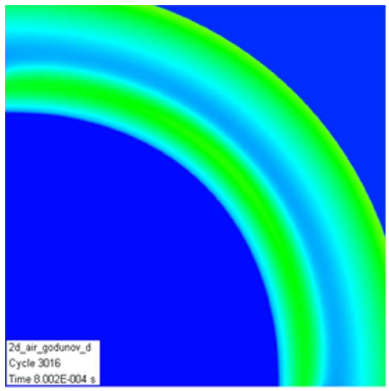

Figure 3.6: Density profiles produced by the Godunov solver in the Richtmyer-Meshkov test at t=0.80ms.

of the advantages of this type of plots is that they more easily can be compared with experimental data often collected using sensors. There is however one fundamental difference between RSPH and the two AUTODYN solvers when it comes to producing sensor data. The latter two are grid solvers where sensor data is obtained by simply extracting the temporal variations at the nearest grid point. Since the computational nodes in RSPH (the particles) move with the fluid flow, additional, immobile sensor points must be defined in order to obtain this kind of data. To find the state at a sensor point, an SPH interpolation must be performed. Any peak values in e.g. density or pressure found by particles infinitely close to a sensor point will, due to the interpolation, lead to a slightly smaller peak on the sensor point. Therefore, slightly lower peak values are typically found when plotting sensor data rather than particle data directly from an RSPH simulation.

In the current set of simulations we have put two sensors along the diagonal, at a distance of 0.5m (sensor 1) and 1.0m (sensor 2), respectively. Figure 3.7 shows the temporal variations in density (top panels) and thermal pressure (bottom panels) found by sensor 1 (left hand panels) and senor 2 (right hand panels) in the RSPH solutions. The black, blue, green, and red lines show the results from simulations **a**-**d**. We see from the left hand plots that the initial shock hits sensor 1 at approximately t=0.12ms. The subsequent contact discontinuity seen at t=0.15ms gives a sharp density peak at sensor 1. At the location of sensor 2, the initial shock arrives at roughly t=0.29ms, while the discontinuity is first detected at t=0.37ms. Based on the arrival times at the sensors, we estimate the average velocities of the fast shock and the contact discontinuity between the two sensors to be 2940m/s (Mach number 8.9 relative to a sound speed of roughly 330m/s) and 2273m/s (Mach number 6.9 relative to a sound speed of roughly 330m/s).

The corresponding FCT sensor data plotted in Figure 3.8 fit quite well with the results of Figure 3.7. One notable difference is the way the two solvers treat the contact discontinuity at sensor 1 in the low resolution limit: Using the RSPH solver, the peak density value is substantially reduce when resolution is reduced. However, the arrival time of the peak remains more or less unchanged, roughly 0.15ms. The peak density value associated with the contact discontinuity does not vary so much between the high and low resolution runs when using the FCT solver. This may in part be because the resolution in RSPH simulation **d** is greater than the corresponding resolution in FCT simulation **d**, with reduced peak density value in the latter simulation as a result. In contrast, the higher peak density values in FCT simulations **a** and **b** compared to that of **RSPH** simulations **a** and **b** are probably an effect of the *flux correction* that tries to compensate for amplitude drops due to numerical dissipation. In addition, there is a distinct trend towards shorter arrival times for the contact discontinuity, when the resolution is reduced. Seen in light of the corresponding RSPH results, it might seem as if the *flux correction* maintains relatively high peak density values at the expense of overestimated propagation speeds. To support this theory, we see that the peak pressure values in the FCT simulations, at both sensors, decrease as resolution increases. Moreover, there is a large degree of agreement between the high resolution peak pressure values found in using the RSPH and FCT solvers. In Figure 3.9, the corresponding sensor data for the Godunov solver have been plotted. It can be seen that the peak density values are much lower than what was the case for the other two solvers, while the peak pressure values agree reasonably well with that shown in

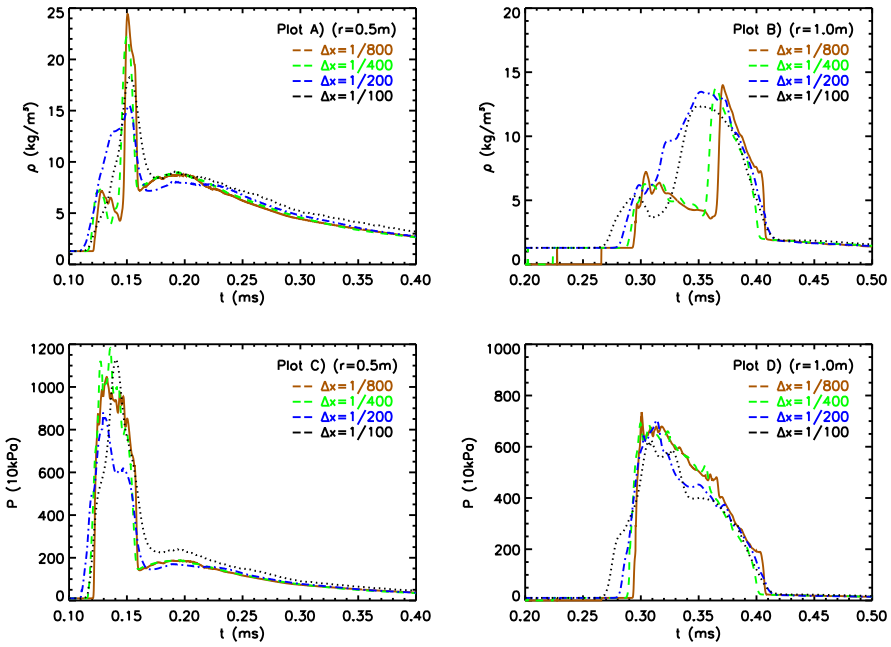

Figure 3.7: Temporal variations in density (top panels) and thermal pressure (bottom panels) as seen by sensor 1 (left hand panels) and sensor 2 (right hand panels) in the RSPH simulations **a-d** *(line colours black/blue/green/red).*

Figures 3.7 and 3.8. Again we see that the Godunov solutions are very smooth with no traces of the small-scale fluctuations seen for the other two solvers. Comparisons of Figures 3.7, 3.8, and 3.9 clearly document the inferior performance of the **Godunov** solver compared to that of the other two solvers.

So far, we have only evaluated the accuracy obtained in concrete simulations in view of the theoretical resolution as indicated by the number of computational nodes. In practice, a more important question is what accuracy can be achieved with a given CPU investment. The answer to this question is obviously not only dependent on the chosen simulation software, but also on the hardware used. All the simulations discussed in this report were run on computers of comparable speed. Although there clearly are some uncertainties connected with such measurements, we believe the CPU-time spent on the different simulations should be more or less directly comparable. The recorded CPU times spent on each of the Richtmyer-Meshkov simulations are given in Table 3.1. We see that the RSPH solver is the faster solver for the simulations **a-c** where the smallest particle size is equal to the grid size. The speed-up increases gradually as the resolution increases from 1.5 to 2.2 when compared to the **Godunov** solver and from 2.0 to 3.4 when compared to the FCT solver. For simulation **d**, the smallest particle size is 1.6 times smaller than the grid size in the corresponding FCT and Godunov simulations. Despite this, the CPU-time of the RSPH simulation is less than the CPU-time of the FCT simulation and only 10% larger than the CPU-time of the Godunov simulation. If the FCT solver had been run with 1600×1600 grid, corresponding to the smallest particle size

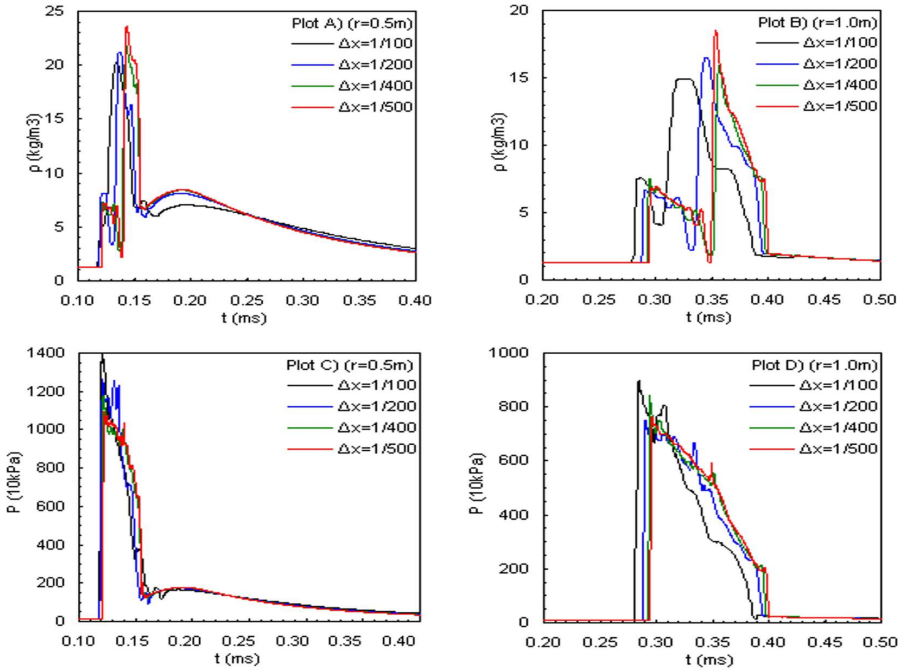

Figure 3.8: Temporal variations in density (top panels) and thermal pressure (bottom panels) as seen by sensor 1 (left hand panels) and sensor 2 (right hand panels) in the FCT simulations **a-d** *(line colours black/blue/green/red).*

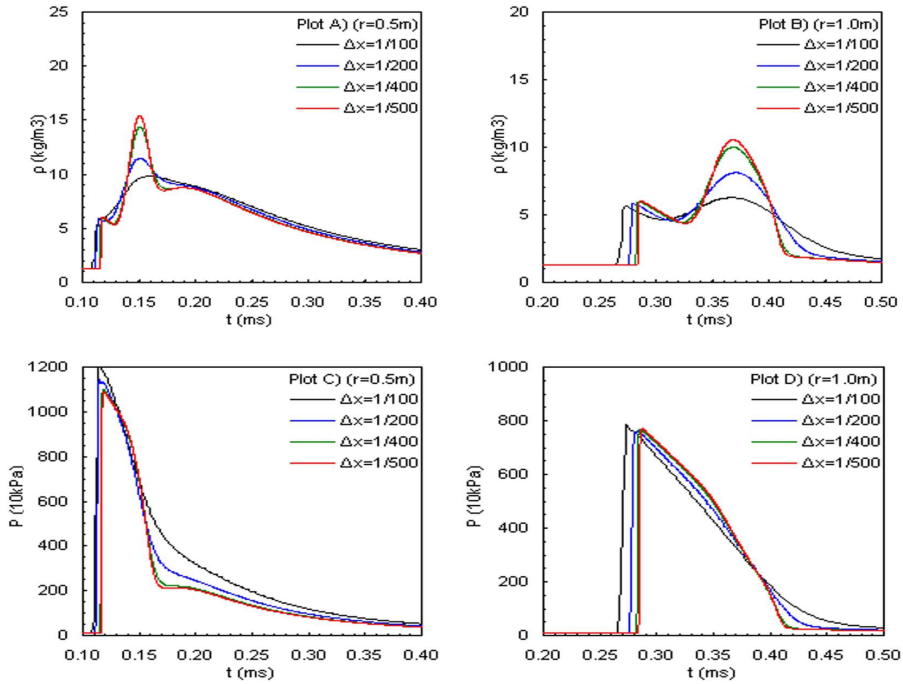

Figure 3.9: Temporal variations in density (top panels) and thermal pressure (bottom panels) as seen by sensor 1 (left hand panels) and sensor 2 (right hand panels) in the Godunov simulations **a-d** *(line colours black/blue/green/red).*

CPU-times for the Richtmyer-Meshkov simulations

Resolution	RSPH	FCT	Godunov
a	4m	8m	6m
b	22m	56m	37m
c	2h 7m	7h 11m	4h 40m
d	12h 35m	15h 7m	10h 16m

Table 3.1: Each entry indicates the CPU-time spent by the RSPH, FCT, and Godunov solvers in simulating the cylindrically shape charge in free field for the full simulation time of 1ms. The four different resolutions are denoted **a**, **b**, **c**, *and* **d**.

in the high resolution RSPH simulation, the CPU-time is estimated to be roughly 62 hours. This estimate is found by extrapolating the increase in CPU-time found between FCT simulations **c** and **d**. It clearly illustrates the benefits of choosing an adaptive numerical solver where resolution can be changed both in time and space.

3.2 Cylindrical charge detonation in plane symmetric chamber

In the next test, we put the charge described in the previous test into a relatively complex, plane symmetric chamber to study how the solvers handle the interactions with solid surfaces and the overall, long-term evolution of the blast waves. This is relevant for studying e.g. accidental detonations inside ammunition storage facilities. The general structure of the chamber is illustrated in Figure 3.10 where the red regions represent walls and cylindrical obstacles in the flow, whereas the black dot situated at x=1m and y=8m indicates the centre of detonation. The chamber consists of an inner chamber to the far left, a channel, an outer chamber with 4 cylindrical pillars, and 3 short blind alleys to the far right. Figure 3.10 also shows how the h-profile typically looks (darker colours indicate smaller h) in the later stages of this simulation. The solid boundaries in the RSPH solver was handled using mirror particles. The sharp corners were treated similarly to that described in [7]. Simulations were run up to 100ms for all three solvers at different resolution levels. However, since the previous tests revealed the Godunov to be distinctly less accurate than the other two solver, we will only report on results obtained with the RSPH and FCT solvers for this test. To simplify the simulation of the initial phase of this problem, the solution has been assumed to be cylindrically symmetric up to the point in time when the primary shock front hits the rear wall. This occurs at time t=0.285ms. The initial phase is solved as a one-dimensional problem in cylinder symmetry. The solution from the one-dimensional problem is then imported into the current, two-dimensional problem. With all three solvers, the simulations started from the same solution at t=0.285ms.

The problem was run 3 times, with a different resolution level each time, using either RSPH or FCT. In the latter case, the problem was solved with 9 (run **a**), 27 (run **b**), and 63 (run **c**) cells per meter. In the RSPH simulations, there are several parameters that effect both the accuracy and

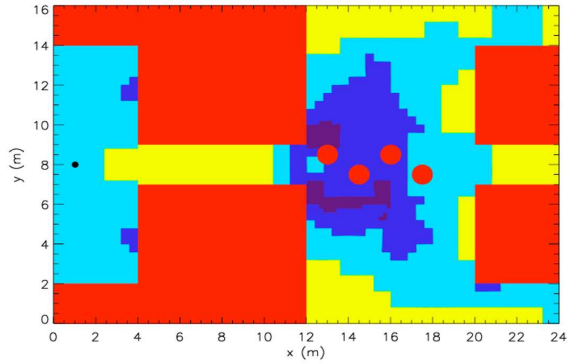

Figure 3.10: Illustration of the chamber layout for the test describing a cylindrical charge in a plane symmetric chamber. Overlayed is the h-profile at time t=40ms.

CPU-times for the Plane Chamber simulations

Resolution	RSPH	FCT
a	4h 24m	13m
b	9h 54m	7h 51m
c	21h 3m	93h

Table 3.2: Each entry indicates the CPU-time spent by the RSPH and FCT solvers in simulating the cylindrically shape charge in the plane symmetric chamber for the full simulation time of 100ms. The three different resolutions are denoted **a**, **b**, *and* **c**.

CPU-time, and the resolution is as indicated in Figure 3.10 highly non-uniform. The time and space averaged particle size in the three simulations were equivalent to 24 (run **a**), 28 (run **b**), and 33 (run **c**) particles per meter. Note that the mean resolution does not change so much between the 3 RSPH simulations as is the case with the 3 FCT simulations. This is naturally reflected in the CPU-time spent on each simulation. The CPU-times are summarized in Table 3.2. Due to the fact that the spread in resolution and CPU-time between the 3 simulations are so much greater in the case of the FCT solver than in the case of the RSPH solver, we will compare RSPH simulations **a** and **c** to the FCT simulations **b** and **c**. From Table 3.2 we see that the CPU-expense of solving the problem with 27 cell per meter using FCT is roughly 78% larger than the CPU-expense when solving the problem with 24 particles per meter on average using RSPH (runs **a** in both cases). As for the high resolution simulations (runs **c**), the FCT CPU-time was 4.4 times larger than the corresponding RSPH CPU-time.

Apart from the fact that the first phase (up to t=0.285ms) is treated by a purely cylindrical description, one would expect that the near field should bear clear resemblance to the free field situation described in the previous section. This implies, that Richtmyer-Meshkov instabilities are likely to play a discernable role also in the present problem. In Figure 3.11 we see the density profile at t=2.5ms in the RSPH simulations **a** (left image) and **c** (right image). In the lower resolution run,

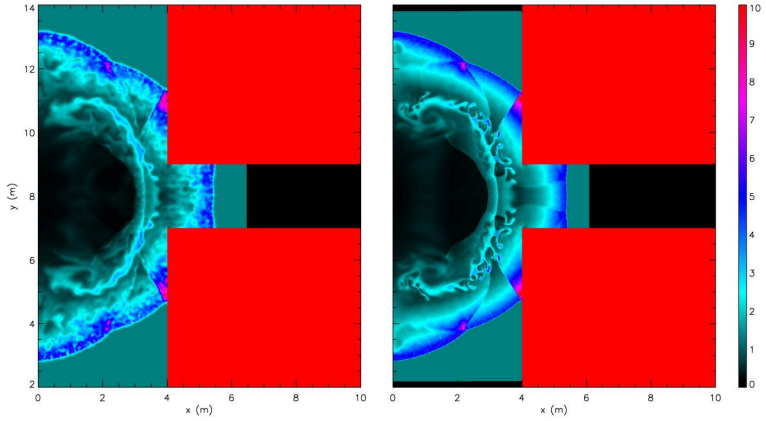

Figure 3.11: Snapshot at t=2.5ms of the density profile in the plane chamber test in the case of the RSPH simulations **a** *(left) and* **c** *(right).*

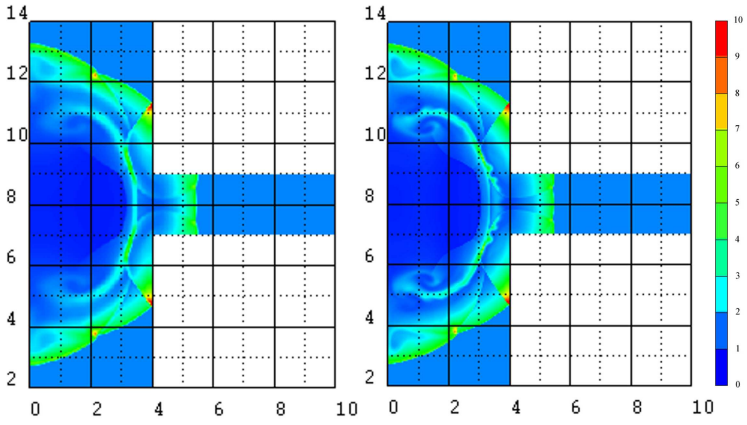

Figure 3.12: Snapshot at t=2.5ms of the density profile in the plane chamber test in the case of the FCT simulations **b** *(left) and* **c** *(right).*

we can only observe weak traces of the instabilities, while in the higher resolution run the characteristic mushroom-like structures are quite well developed. We also notice that the noise level in the region right behind the primary shock is considerably higher in the lower resolution simulation. Nevertheless, they both capture more or less the same main features. The corresponding images from the FCT simulations are found in Figure 3.12. We see that the lower resolution simulation (left image) in this case show no traces of the Richtmyer-Meshkov instabilities. Even the high resolution results of Figure 3.12 reveal little from the weak traces found in the lower resolution results of Figure 3.11. Yet, the main features in Figure 3.12 still fit well with that found in Figure 3.11. To better study quantitative difference between the 4 solutions we have also included horizontal cuts through the density profiles along the mid plane of the chamber, at y=9m. Figure 3.13 shows, from left to right, the FCT simulations **b** and **c** (left pair of panels), and the RSPH simulations **a** and **c** (right pair of panels. These graphs confirm that there is a large degree of consistency between the solutions obtained with the two different solvers. The most notable difference is the double peak

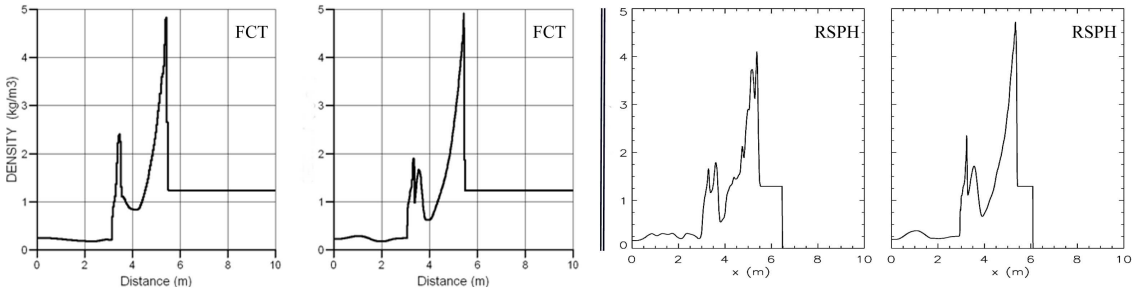

Figure 3.13: Horizontal cut through the density profile at the mid plane and t=2.5ms in the plane chamber test. Plotted from left to right are the profiles from the FCT simulations **b** *and* **c**, *and RSPH simulations* **a** *and* **c**. *Note that the RSPH profiles drop to 0 in the interval (x>6-6.5m) where no particles are found.*

at roughly x=3-3.5m which in the lower resolution FCT simulations is a single peak with enhanced amplitude. Note also that the reason why the RSPH profiles drop to zero at roughly x=6m is because no computational nodes have been generated at this point in time for x larger than roughly 6m.

In the beginning of the simulation, the state of the system changes rapidly. At t=5.0ms, the fast shock wave has already reached almost half-way through the channel and the shock wave patterns have become quite complicated due to multiple reflections from the chamber walls. This is shown through colour images of the density profile in Figures 3.14 and 3.15 for the RSPH and FCT solvers, respectively. At this point in time, a shock focus has occurred in the right corners of the inner chamber. Other than this, the inner chamber is dominated by the weakened remains of the instabilities creating thin filaments of increased density in the high resolution RSPH simulation. In the other 3 simulations, these filaments are thicker and with less details to them. This applies in particular to the low resolution FCT results. Also, we can already at this early stage begin to notice the main distinction between the RSPH and the FCT results: The shocks are propagating faster in the FCT simulations. This is most easily seen by studying the shock wave pattern at around x=6m in the two high resolution results. The horizontal cuts through the mid plane, shown in Figure 3.16, reveal the peak density to be slightly higher in the RSPH than in the FCT results. In this regard, please note that the density range shown on the y-axis is not the same on all 4 panels. Apart from this, the 4 results can still be considered highly consistent with each other. Again, the RSPH profiles drop to zero in part of the plotted interval (x larger than roughly 8.5m) because no particles have yet been generated in this part of the domain.

At time t=15ms the fast shock waves are seen in Figures 3.17 and 3.18 to have propagated through the tunnel, expanded into the outer chamber and reflected off the first two pillars. The reason for including the pillars in this model was to see how well the solvers could handle the curved surfaces. We can conclude that both RSPH and FCT treat this satisfactorily. Looking at the horizontal cuts through the mid plane of the density profiles, as shown in Figure 3.19, we see however that the differences between the 4 solutions are starting to become more evident. Note that what appears

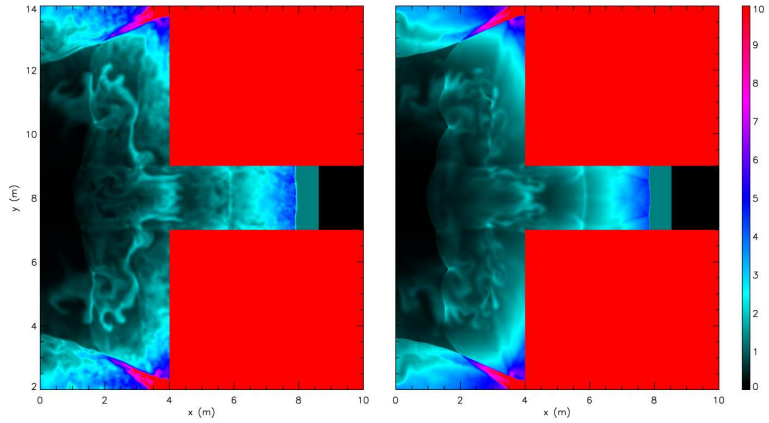

Figure 3.14: Snapshot at t=5.0ms of the density profile in the plane chamber test in the case of the RSPH simulations **a** *(left) and* **c** *(right).*

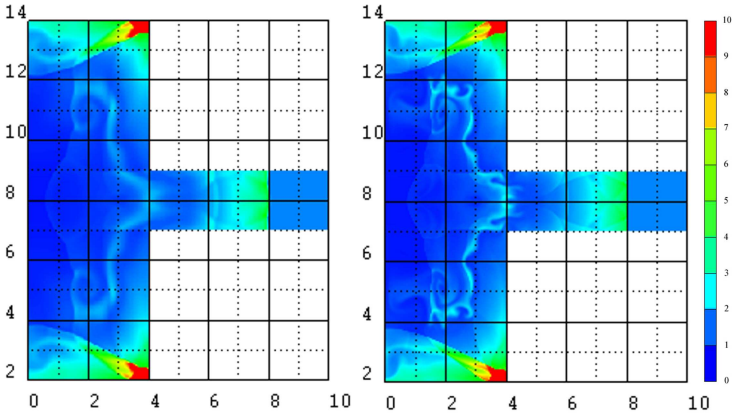

Figure 3.15: Snapshot at t=5.0ms of the density profile in the Plane Chamber test in the case of the FCT simulations **b** *(left) and* **c** *(right).*

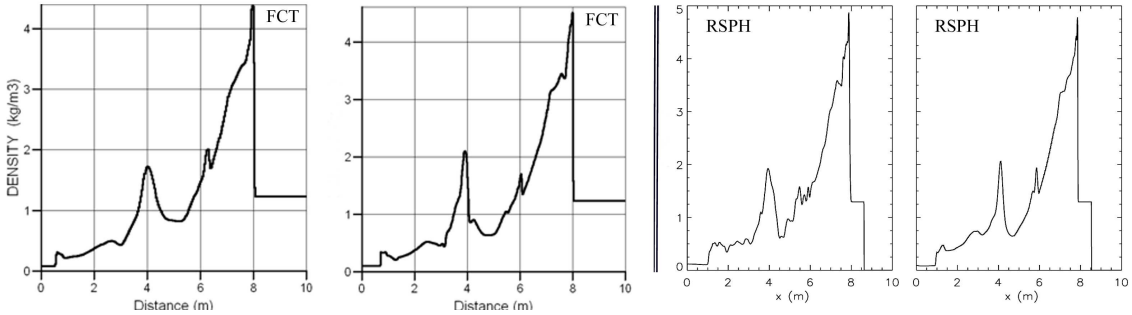

Figure 3.16: Horizontal cut through the density profile at the mid plane and t=5.0ms in the plane chamber test. Plotted from left to right are the profiles from the FCT simulations **b** *and* **c**, *and RSPH simulations* **a** *and* **c**.

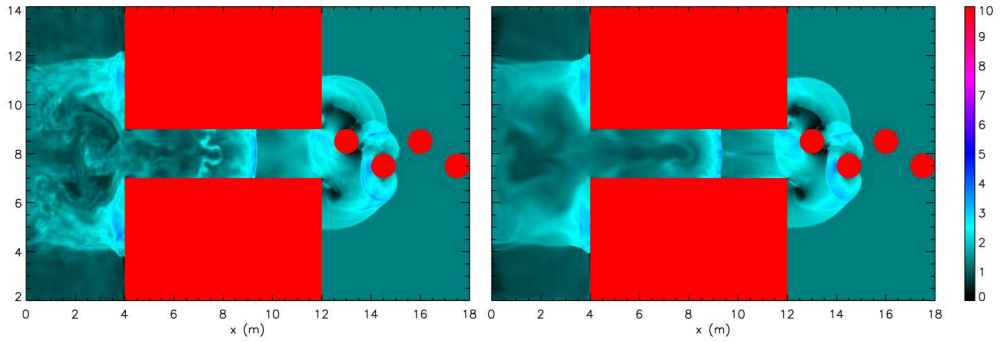

Figure 3.17: Snapshot at t=15ms of the density profile in the plane chamber test in the case of the RSPH simulations **a** *(left) and* **c** *(right).*

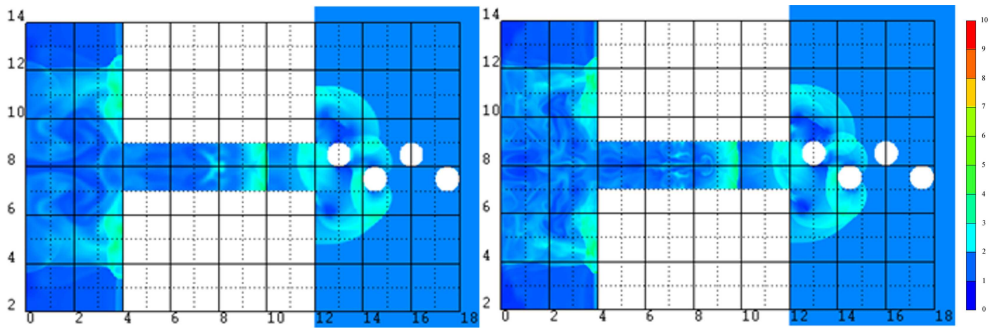

Figure 3.18: Snapshot at t=15ms of the density profile in the Plane Chamber test in the case of the FCT simulations **b** *(left) and* **c** *(right).*

to be a density maximum in the RSPH results at x=14.5m and density minima in the FCT results at x=13m and x=15.5m are artificial plotting effects due to the horizontal cuts grazing the pillar surfaces. However, the peak found near x=10m is genuine and can be used to compare the different solutions. The FCT solutions give a slightly faster propagation speed, as noted before. The peak value, on the other hand, is larger by some 25% in the high resolution RSPH results compared to that of the other results. In contrast, the density profile in this simulation has by now much less distinct features in the region behind this peak. This is because the particular choice of parameters for this simulation gave a more non-uniform resolution profile in simulation **c** compared to simulation **a**.

By the time the simulation reaches t=20ms, the difference in propagation speeds between the RSPH and FCT solutions has accumulated to a noticeable difference in shock positions, as seen in Figures 3.20 and 3.21. In particular, this is easily seen by comparing how much of the fast shock has reflected off the last pillar. At this point, we estimate the shock speeds in the FCT results to be roughly 2-3% higher than the corresponding speeds in the RSPH results. Other differences seen by comparing the images of Figures 3.20 and 3.21 can in part be due to differences in the colour tables used. However, the horizontal cuts at t=20ms, shown in Figure 3.22, show much the same tendency as before, namely that the primary peak found roughly at x=12m is stronger in the RSPH results. A

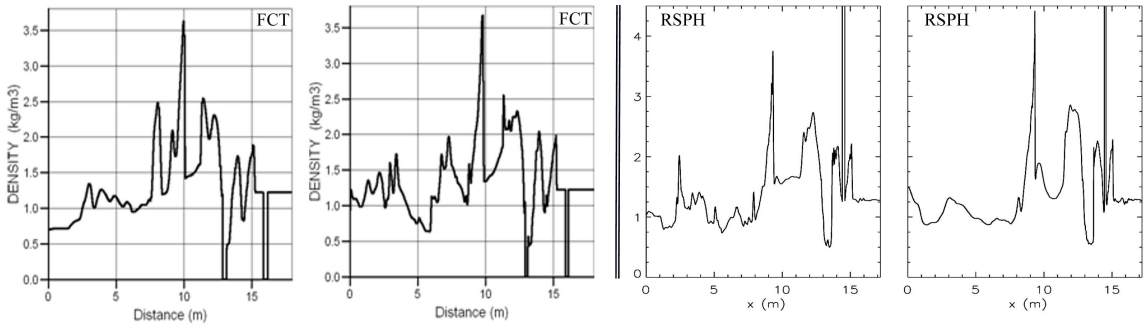

Figure 3.19: Horizontal cut through the density profile at the mid plane and t=15ms in the plane chamber test. Plotted from left to right are the profiles from the FCT simulations **b** *and* **c**, *and RSPH simulations* **a** *and* **c**.

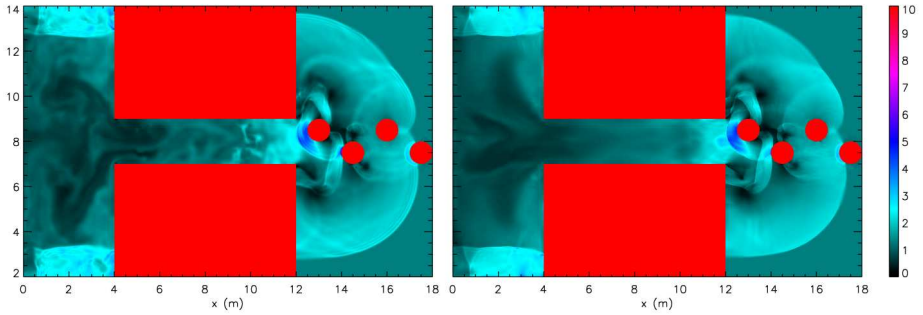

Figure 3.20: Snapshot at t=20ms of the density profile in the plane chamber test in the case of the RSPH simulations **a** *(left) and* **c** *(right).*

secondary peak, found at x $\approx$ 14m, is on the other hand stronger in the high resolution FCT results. However, this peak has a rapidly increasing amplitude so that even small time shifts can play an important role. The smaller propagation speed in the RSPH results thus makes the secondary peak not as evolved as the corresponding peak in the FCT results at a given point in time.

At t=40ms the asymmetries in the pillar positions have become a dominating factor in determining the evolution of the flow. From Figures 3.23 and 3.24 we see that air has been more easily channeled towards the lower blind alley compared to the upper blind alley. In the RSPH results, the fast shock is just about to hit the back wall of the lower blind alley, whereas in the FCT results, the reflected shock is already on its way back. Studying closely the two images of Figure 3.24 we can also detect a slight difference in the position of the shock waves in the lower and upper blind alleys. More specifically, we see that the propagation speeds are slightly higher in lower resolution results. The difference in timing between the two FCT results are still much smaller than the difference in timing between the high resolution FCT and RSPH resolution. The later stages of the simulation is dominated by a rather turbulent flow field as can be seen from Figures 3.25 and 3.26 at t=80ms. This is primarily due to the fairly large number of vortices generated as gas passes near surface corners or near the cylindrical pillars. When these vortices interact with the reflected shocks the

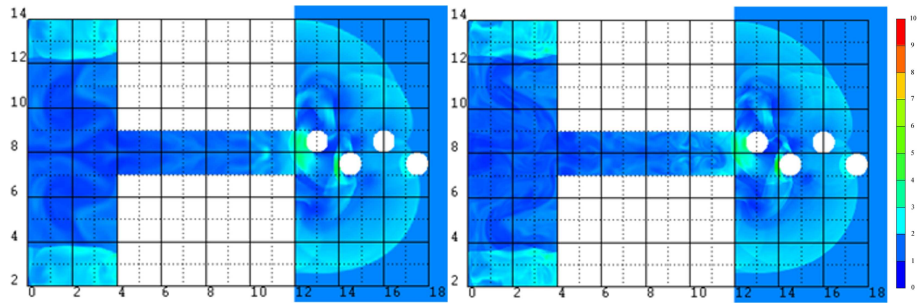

Figure 3.21: Snapshot at t=20ms of the density profile in the plane chamber test in the case of the FCT simulations **b** *(left) and* **c** *(right).*

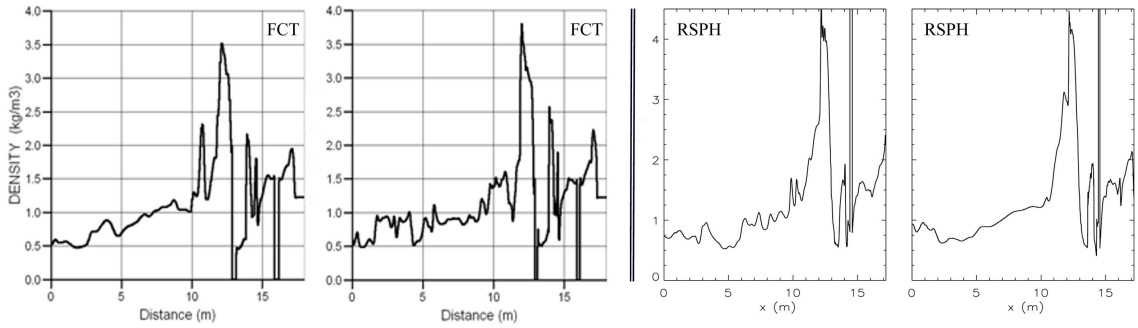

Figure 3.22: Horizontal cut through the density profile at the mid plane and t=20ms in the plane chamber test. Plotted from left to right are the profiles from the FCT simulations **b** *and* **c**, *and RSPH simulations* **a** *and* **c**.

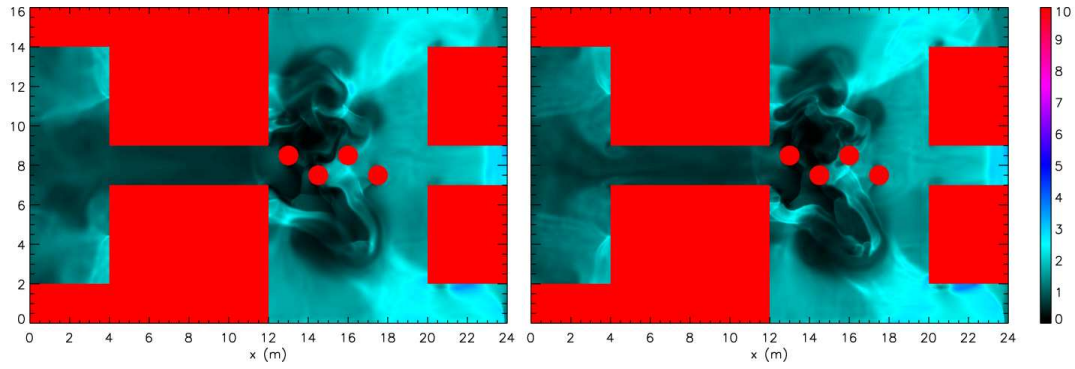

Figure 3.23: Snapshot at t=40ms of the density profile in the plane chamber test in the case of the RSPH simulations **a** *(left) and* **c** *(right).*

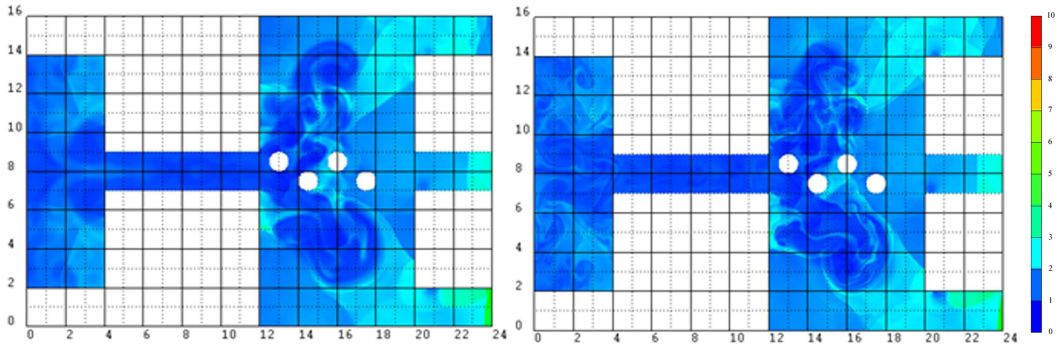

Figure 3.24: Snapshot at t=40ms of the density profile in the plane chamber test in the case of the FCT simulations **b** *(left) and* **c** *(right).*

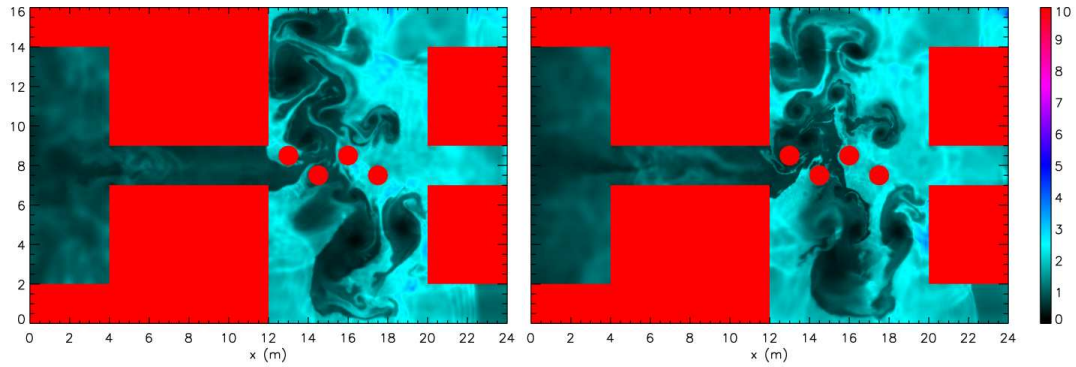

Figure 3.25: Snapshot at t=80ms of the density profile in the plane chamber test in the case of the RSPH simulations **a** *(left) and* **c** *(right).*

turbulence grows. As is expected with turbulent flows, the detailed flow pattern will not be the same in simulations where the resolution or solving method is not the same.

4 A cylindrically symmetric test

It is sometimes useful to apply a two-dimensional, cylindrically symmetric description to a problem. In this way, simulations of e.g. spherical charges detonated in cylindrical chambers can be studied using a two-dimensional model. Non-Cartesian formulations of SPH related methods are not commonly used. However, a formulation adapted in the RSPH code has recently been developed and tested [15, 17]. The test which will be the focus of this section is described in [16]. In fact, the RSPH results presented here have already been partially reported in [16]. The FCT and Godunov results presented here have not been published before. All three solvers use a one-dimensional, spherical model to describe the evolution of the system up to t=0.40ms. From this point on, the simulations are carried out in two-dimensional cylindrical coordinates. The maximum resolution in the RSPH

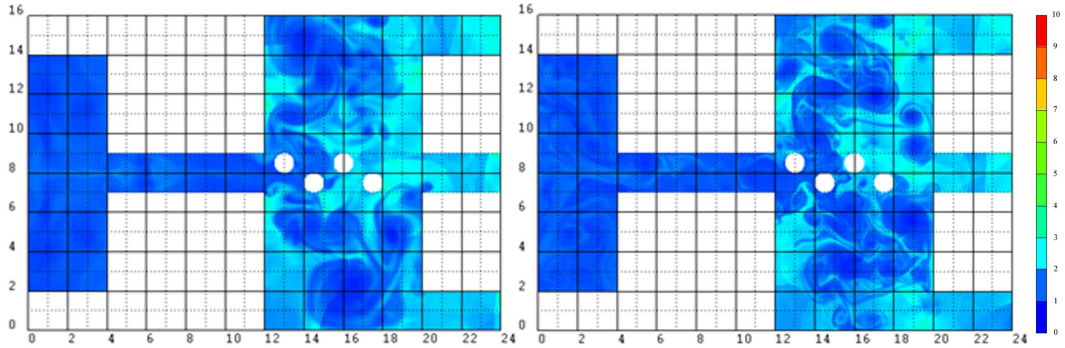

Figure 3.26: Snapshot at t=80ms of the density profile in the plane chamber test in the case of the FCT simulations **b** *(left) and* **c** *(right).*

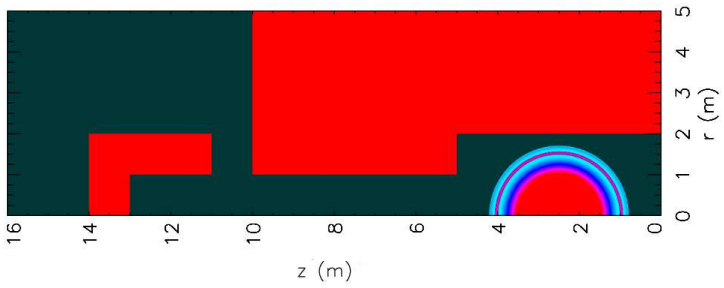

Figure 4.1: Illustration of the chamber layout for the test describing a spherical charge in a cylindrically symmetric chamber. Overlayed is the density profile at time t=40ms.

simulation is 160 particles per meter and a smoothing length of 1.25cm. In comparison, the FCT and Godunov results are obtained with 80 and 63 cells per meter, respectively. These are, in other words, resolution levels similar to what was used in the previous test.

This test applies the same material properties as that used in chapter 3. This means that the charge consists of TNT with a mass density of $1630\text{kg}/\text{m}^3$ and a specific energy of 4.29MJ/kg, while the air is assumed to have a density of $1.293\text{kg}/\text{m}^3$ and a pressure of 1 atm. This time, the charge is assumed to be spherical with a radius of 358mm. The charge is placed in a cylindrical chamber, on the symmetry axis at z=2.5m. The outline of the chamber is illustrated in Figure 4.1. The chamber consists of an inner and outer chamber, both with a height of 5m and with radius of 2m and 1m, respectively. At z=10m, the chamber entrance is found, however a u-shaped barrier is situated in front of the opening so as to obstruct the flow of shock waves coming out. The solid surfaces are coloured red in Figure 4.1. The figure also shows the density profile at t=0.40ms, which marks the start of the two-dimensional simulation.

Due to the larger HE charge used in this test relative to that of the plane symmetric tests presented in 3, the temporal evolution is expected to be more rapid. This is confirmed by the simulated results. In the left pair of panels of Figure 4.2 we see the density profile at time t=1ms in the RSPH (panel

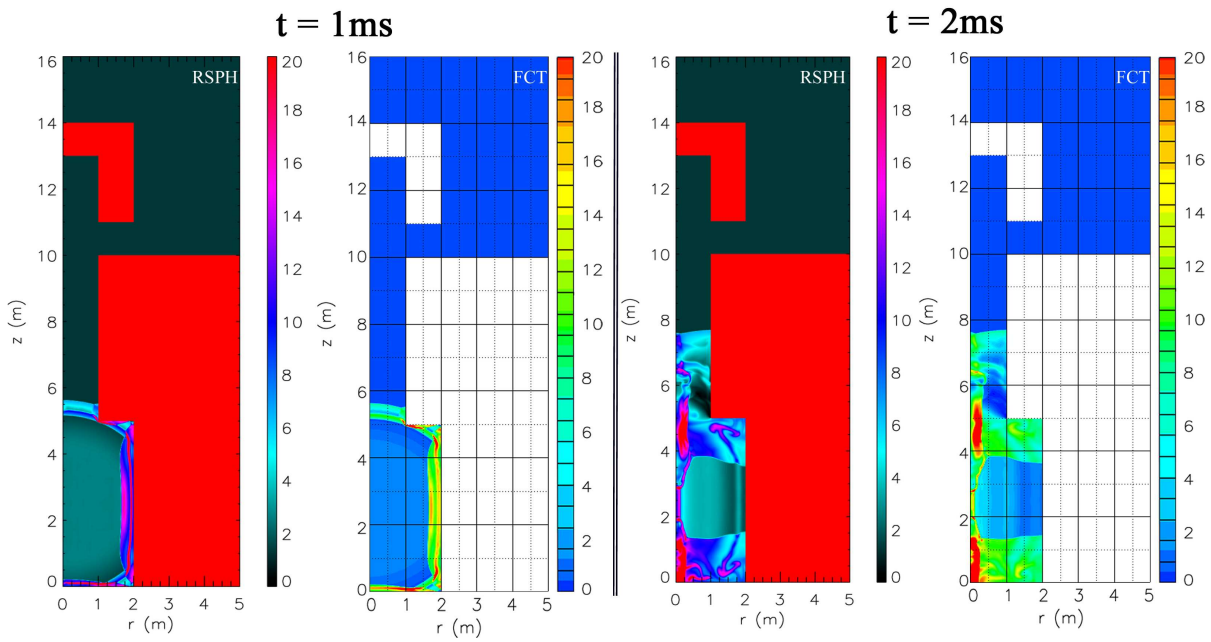

Figure 4.2: Snapshots of the RSPH (panels 1 and 3 from the left) and FCT (panels 2 and 4 from the left) solutions at times t=1ms (left pair of panels) and t=2ms (right pair of panels) of the test describing a spherical charge in a cylindrical chamber.

1) and FCT (panel 2) solutions. In both solutions the originally spherical blast wave has reflected off the chamber floor, as well as the inner chamber wall and the corner marking the start of the outer chamber. At time t=2ms the density profiles, shown in the right pair of panels of Figure 4.2, have already become quite complicated due to the many reflections. A Mach reflection has evolved near the symmetry axis at the position of the fast shock front, which as this point in time is located roughly midway through the outer chamber. Despite the differences in colour schemes, we clearly see that there is quite a large degree of agreement between the two solvers. Looking more closely though, we can notice a few differences: The thin, high-density layer found in the inner chamber at t=1ms and radius roughly 2.8m has a more uniformly high density in the RSPH solution. In the FCT solution, this structure is strongly dominated by peaks near the bottom and top ends of the layer. The radial position of the layer seems to indicate a somewhat higher propagation speed in the FCT solution than in the RSPH solution. At t=2ms we notice that the RSPH solution has clearly visible mushroom-like structures at r $\sim$ 1.5m near the bottom and top of the inner chamber. From the plane symmetric test of chapter 3 we recognize these as signatures of instabilities. These structures are not to the same extent visible in the FCT solution.

From Figure 4.3, where the density profiles at times t=3ms (left pair of panels) and t=4ms (right pair of panels) are plotted, we see that the instabilities in the inner chamber continue to evolve in the time frame up to 4ms. At this stage, the FCT solutions (panels 2 and 4 from the left) has also started to show traces of instabilities, although not to the same extent as in the RSPH solutions (panels 1 and 3 from the left). At the front, there is also a noticable difference between the two solutions. The

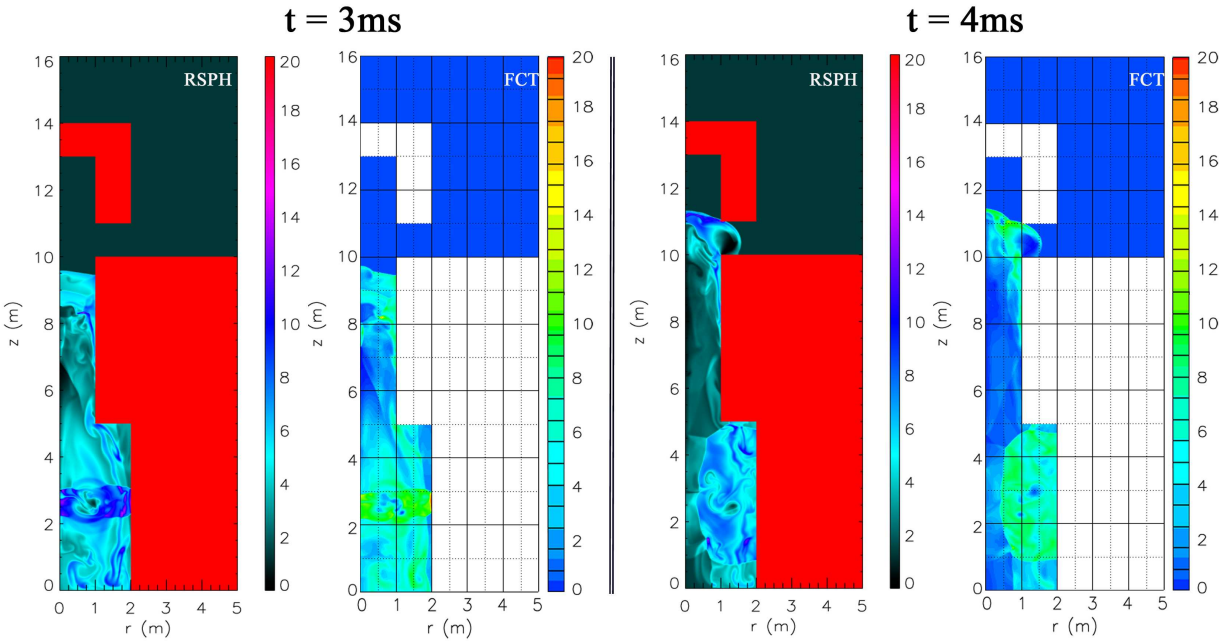

Figure 4.3: Snapshots of the RSPH (panels 1 and 3 from the left) and FCT (panels 2 and 4 from the left) solutions at times t=3ms (left pair of panels) and t=4ms (right pair of panels) of the test describing a spherical charge in a cylindrical chamber.

FCT solution seems to have an extra triple point compared to the corresponding RSPH solution. At time t=4ms, this triple point is still present in the FCT solution only. The high density region behind the fast shock front, on the other hand, is larger in the RSPH solution than in the FCT solution. The origin of these differences is not known, but it is unlikely that this is related to any differences in propagation speed.

So far we have only compared the RSPH and FCT solutions, and we see that there is a fairly high degree of consistency between the two solutions. In Figures 4.4 and 4.5 we have compared all three solvers, including the Godunov solver. Figure 4.4 consists of 8 different panels, labelled **a-h** for convenience. These panels show cuts at r=0.1m through the density (**a-d**) and pressure (**e-h**) profiles in the RSPH (blue line), FCT (red line), and Godunov (green line) solutions at times t=1ms, 2ms, 3ms, and 4ms. We quickly note the Godunov solution exhibits much lower peak densities at t=1ms, shown in panel **a**. At z $\sim$ 5.5m, the RSPH and FCT solvers agree quite well on the peak densities, while near z=0m the FCT solution is somewhere between the Godunov and RSPH solutions. The pressure profile, shown in panel **e**, reveal that the three solvers agree more or less on the pressure profile at $z \sim 5.5$m, but that the Godunov solver shows much higher peaks than the other two solvers near z=0m. Already at time t=2ms, shown in panels **b** and **f**, we see that the Godunov solver gives a dramatically different solution to the other two solvers. The peak values, both in density and pressure, are in general much lower in the Godunov solution than what is seen from the other two solutions. In particular the short wave length perturbations seem to be missing from the Godunov solution. In fact, the only structure in the profile that seems to be reproduced at

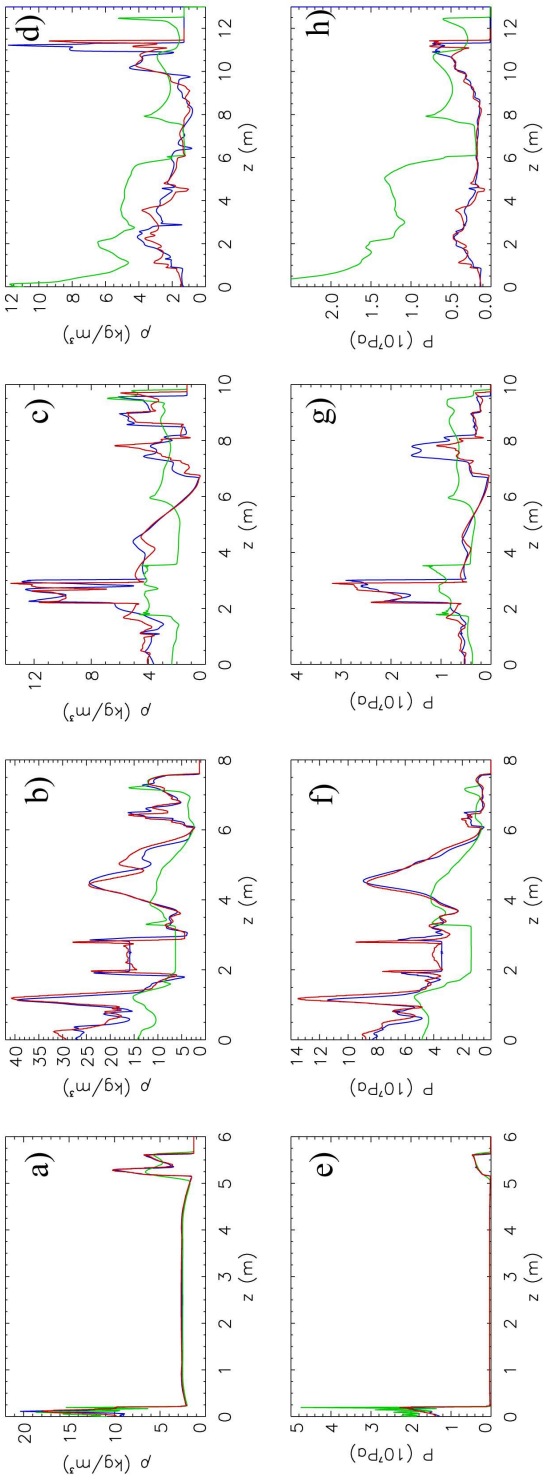

Figure 4.4: Cuts along the symmetry axis at a distance of 10cm and, from left to right, at times t=1ms, 2ms, 3ms, and 4ms. The upper panels show the density profiles, while the lower panels show the pressure profiles. The green, red, and blue lines depict the Godunov, FCT, and RSPH solutions, respectively.

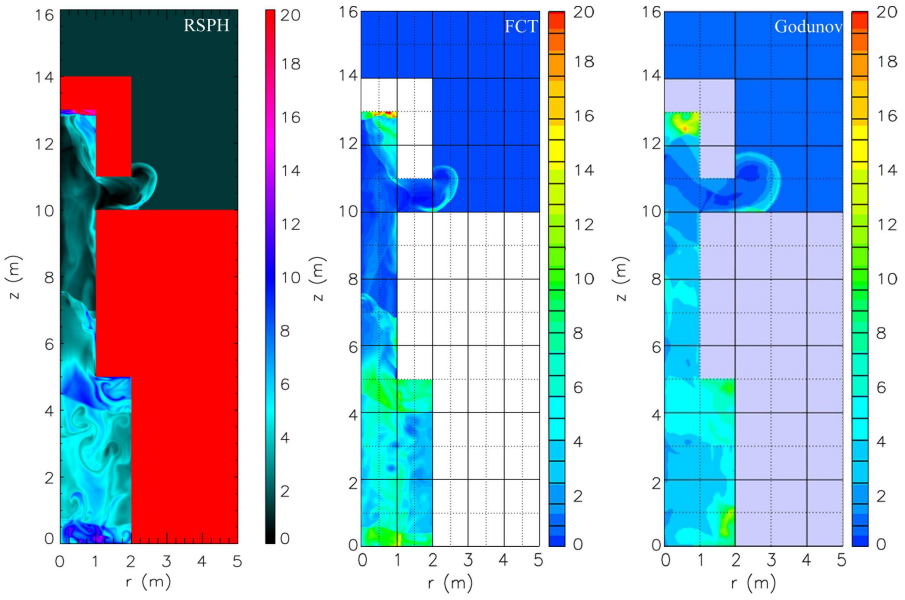

Figure 4.5: Snapshots of, from left to right, the RSPH, the **FCT**, *and the Godunov solutions at time t=5ms of the test describing a spherical charge in a cylindrical chamber.*

this point is the position of the fast shock front (z $\approx$ 7.5m).

For the last two pairs of profiles, at times t=3ms (panels **c** and **g**) and t=4ms (panels **d** and **h**), we see that the difference between the Godunov solution and the other two solutions steadily increases. Even the RSPH and FCT are by now showing clear indications of differences, as we have already seen in Figure 4.3. The position of the fast shock front is no longer the same in the three solutions. The shock propagates distinctly faster in the Godunov solution, while the shock in the RSPH solution runs slightly slower than the FCT solution. In Figure 4.5 we see the full density profile in all three solutions plotted at time t=5ms. At this point in time, the fast shock is about to leave the chamber altogether. The shock has clearly propagated the farthest in the Godunov solution. The overall level of details are also much less in this solution. The differences between the RSPH and FCT solutions are harder to spot, but a number of details, such as the presence and position of triple points, vortices, and mushroom-like structures are no longer the same in the two solutions. To the extent that turbulent flows have evolved, one would of course not expect the details of the two solutions to match. However, there also seems to be a difference in the *level* of turbulence between the two solutions. Overall, there seems to be a fundamental difference between the RSPH and FCT solutions on one side and the Godunov solution on the other side, and it seems as if this difference might be connected with the way the shock-boundary interactions are described in the Godunov solver. This indication of malfunction was recently reported to the AUTODYN developing team at ANSYS and the behaviour was confirmed by tests done by their group. The behaviour seems to be coupled to environments of extremely high pressure. Other than that, no explanation has of yet been found.

5 Conclusion

In this report, we have compared the SPH based code RSPH with two solvers, the Godunov and FCT solvers, found in the commercially available hydro-code AUTODYN on problems involving blast waves in one- and two-dimensional geometries. This kind of comparative study is not only essential when developing new numerical codes such as the RSPH code. It is also very useful in assessing the reliability of commercial codes, such as AUTODYN. Due to commercial interests, software companies may not be so eager to publish results from in-depth comparisons with other available software packages. In fact, we are not aware of any published studies where the capabilities of AUTODYN to simulate compressible fluid flows have been compared directly with that of other numerical codes. We therefore believe that, to the extent that AUTODYN is indeed applied to this class of problems, a study such as the present is highly useful.

The test results presented in this report can be summarized as follows: The RSPH and FCT solvers are distinctly more accurate than the Godunov solver in all tests. In general, the results from the latter solver are dominated by excessive numerical dissipation, leading to artificial damping of instabilities and reduced density amplitudes. As particularly well illustrated by the results from the Richtmyer-Meshkov test in chapter 3.1, the sound speed in the shocked gas increases when resolution is reduced. This leads to an overestimation of the shock speeds. As noted in [24], this can be an indication of lack of numerical conservation (e. g. momentum and total energy). The Richtmyer-Meshkov test also revealed that the Godunov solver is not capable of capturing the instabilities that are important when describing material mixing. The cylindrical test in chapter 4 also shows the Godunov results to be radically different from that of the other two solvers. This can partly be due to the fact that since the propagation speeds are too large, the interaction of different reflected shocks will be different. In addition, an unknown source of error seems be present that causes the pressure near the z=0 boundary to be overestimated by more than a factor of two. This behaviour has later been confirmed by the AUTODYN developing team. This result could be particularly interesting seen in light of the findings in [22]. On the positive side, it can be noted that Godunov is the faster one of the two AUTODYN solvers, by roughly 30%.

The FCT solver is more accurate than the Godunov solver. It seems to deliver surprisingly accurate estimates of peak amplitudes at medium resolution level. This is probably due to the applied flux-correction technique. However, it is possible that the FCT shares the tendency found with the Godunov solver of overestimating the propagation speeds at low resolution, although the level of overestimation is much smaller in the case of FCT. Compared to the RSPH solver, we have identified slightly higher propagation speeds with the FCT solver. In the plane chamber test, the difference in propagation speeds were of the order of a few percent. Other than this, FCT has been shown to be the slower solver of the three, roughly a factor 2-3 times slower than the RSPH solver (when the latter solver is using an adaptive approach). The RSPH solver benefits greatly from the adaptive approach, both in terms of accuracy and efficiency. However, it should be noted that peak amplitudes seem to drop off more quickly when the resolution is reduced compared to FCT. On the other hand, we have not seen any indication that the propagation speeds are greatly affected by a moderate reduction

in resolution. With regards to the observed differences in propagation speeds between the RSPH and AUTODYN solvers, it is worthwhile mentioning a recent study where cylindrically symmetric simulation results from RSPH has been found to be highly consistent with corresponding results from the numerical code Chinook as well as experimental data [18].

This report not only underlines the benefits from having access to a non-commercial, state-of-the-art numerical code as a means for validating other codes as well as gaining new insight into the fundamental physics of detonation. Maybe even more important, is the new insight into the performance of a specific numerical tool, namely AUTODYN. This is insight which is essential in interpreting the results obtained with the code. The Godunov solver has so far been preferred in many situation over the FCT solver because it offers more possibilities in modelling multi-material problems and are the faster solver. Unfortunately, this work indicates that the Godunov solver is not what one with today's standards would call a highly accurate method. (There are many accurate Godunov schemes being used in other codes. However, these are **higher order** Godunov schemes.) On a more general note, one can say that both [2] and the present work demonstrates the importance of knowing the limitations of the software tools in use and of running simulations with sufficient resolution.

References

[1] Benz, W. & Asphaug, E.: **Simulations of brittle solids using smoothed particle hydrodynamics**, Comput. Phys. Commun. 87, 253, 1995

[2] Bjerke, A., Teland, J. A. & Svinsås, E.: **Modelling of complex urban blast scenarios using the AUTODYN hydrocode**, FFI/RAPPORT-2008/02096, 2008

[3] Boris, J. P. & Book, D. L.: **Flux-corrected transport: I. SHASTA, a fluid transport algorithm that works**, J. Comput. Phys. 11, 38, 1973

[4] Børve, S., Omang, M., & Trulsen, J.: **Regularized smoothed particle hydrodynamics: A new approach to simulating magnetohydrodynamic shocks**, Astrophys. J. 561, 82, 2001

[5] Børve, S., Omang, M., & Trulsen, J.: **Regularized smoothed particle hydrodynamics with improved multi-resolution handling.**, J. Comput. Phys. 208, 345, 2005

[6] Colagrossi, A. & Landrini, M.: **Numerical simulation of interfacial flows by smoothed particle hydrodynamics**, J. Comput. Phys. 191, 448, 2003

[7] Colagrossi, A., Colicchio, G., & Le Touzé, D., **Enforcing boundary conditions in SPH applications involving bodies with right angles**, Proc. 2nd SPHERIC Workshop, Madrid, Spain 59, 2007

[8] Gingold, R. & Monaghan, J. J.: **Theory and applications to non-spherical stars**, Mon. Not. R. Astron. 181, 375, 1977

[9] Godunov, S. K.: **A finite difference method for the numerical computation and discontinuous solutions of the equations of fluid dynamics.**, Math. Sbornik, 47, 271, 1959

[10] Jones, M. A. & Jacobs, J. W.: **A membraneless experiment for the study of Richtmyer-Meshkov instability of a shock-accelerated fas interface**, Phys. Fluids 9, 3078, 1997

[11] Klomfass, A.: **Numerical investigation of fluiddynamic instabilities and pressure fluctuations in the near field of a detonation**, Proc. 20th Int. Symp. Military Aspects of Blast and Shock, Oslo, Norway 2008

[12] Mikaelian, K. O.:**Growth Rate of the Richtmyer-Meshkov Instability at Shocked Interfaces**, Phys. Rev. Lett. 71, 2903, 1993

[13] Meshkov, E. E.: **Instability of a shock wave accelerated interface between two gases**, NASA Tech. Trans. F-13, 074, 1970

[14] Monaghan, J. J.: **Smoothed particle hydrodynamics**, Rep. Prog. Phys. 68, 1703, 2005

[15] Omang, M., Børve, S., & Trulsen, J.: **SPH in spherical and cylindrical coordinates**, J. Comput. Phys., 213, 397, 2006

[16] Omang, M., Børve, S., & Trulsen, J.: **Modelling High Explosives (HE) using Smoothed Particle Hydrodynamics**, Proc. 26th Int. Symp. Shock Waves, Göttingen, Germany 2007

[17] Omang, M., Børve, S., Christensen, S. O., & Trulsen, J.: **Symmetry assumptions in SPH**, Proc. 2nd SPHERIC Workshop, Madrid, Spain 103, 2006

[18] Omang, M., Christensen, S. O., Børve, S., & Trulsen, J.: **Height of burst explosions, a comparative study of numerical and experimental results**, Shock Waves, submitted, 2008

[19] Richtmyer, R. D.: **Taylor instability in shock acceleration of compressible fluids**, Commun. Pure. Appl. Math. 13, 297, 1960

[20] Samtaney, R. & Meiron, D. I.:**Hypervelocity Richtmyer-Meshkov instability**, Phys. Fluids 9, 1783, 1997

[21] Sharp, D. H.: **An overview of Rayleigh-Taylor instability**, Physica D 12, 3, 1984

[22] Teland, J. A. & Wasberg, C. E.: **A Two-stage approach to numerical simulation of detonation inside an underground ammuntion storage**, FFI/RAPPORT-2006/03221, 2006

[23] Woodward, P. & Colella, P.: **The Numerical Simulation of Two-Dimensional Fluid Flow with Strong Shocks**, J. Comput. Phys. 54, 115, 1984

[24] Xiao, F.: **Unified formulation for compressible and incompressible flows by using multi-integrated moments I: one-dimensional inviscid compressible flow**, J. Comput. Phys. 195, 629, 2004

[25] Zhang, Q. & Graham, M. J.: **A numerical study of Richtmyer-Meshkov instability driven by cylindrical shocks**, Phys. Fluids 10, 974, 1998